1989

High temperature X-ray diffraction and Landau theory investigation of order-disorder transition in defect NaCl-type solids

Sung Jin Kim
Iowa State University

Order Number 9003539

High temperature X-ray diffraction and Landau theory investigation of order-disorder transition in defect NaCl-type solids

Kim, Sung Jin, Ph.D.

Iowa State University, 1989

U·M·I
300 N. Zeeb Rd.
Ann Arbor, MI 48106

High temperature X-ray diffraction and Landau theory investigation of order-disorder transition in defect NaCl-type solids

by

Sung Jin Kim

A Dissertation Submitted to the
Graduate Faculty in Partial Fulfillment of the
Requirements for the Degree of
DOCTOR OF PHILOSOPHY

Department: **Chemistry**
Major: **Physical Chemistry**

Approved:

Signature was redacted for privacy.

In Charge of Major Work

Signature was redacted for privacy.

For the Major Department

Signature was redacted for privacy.

For the Graduate College

Iowa State University
Ames, Iowa

1989

TABLE OF CONTENTS

GENERAL INTRODUCTION

A number of compounds of transition metals with nonmetals of group V and VI with ideal stoichiometric ratio X/M=1 have the NaCl-type crystal structure and have wide ranges of homogeneity resulting from vacancies. These vacancies play an important role in the structural chemistry and electronic properties of these refractory solids.

Research in the area of structure in nonstoichiometric systems is an active and rapidly advancing area of solid state chemisty. For several decades, defects in crystals have been treated as a deviation of the ideal composition of a crystal. A small amount (less than 10%) of vacancies is usually stabilized by the configurational contribution to the entropy.[1] However it is well known that many nonstoichiometric compounds can not be categorized according to this well-established concept of solid state chemistry because the stoichiometric deviation is too wide to be idealized with classical defect theory. Furthermore the vacancies in these solids are observed to order when samples are cooled slowly. Examples of highly defective compounds are $Zr_{1-x}S$ (23% of the metal sites are unoccupied), $Sc_{1-x}S$ (20% of the metal sites are unoccupied),[2] $Lu_{1-x}S$ (25% of the metal sites are unoccupied), NbO (25% of the metal and nonmetal sites are unoccupied), TiO (15% of the metal sites and nonmetal sites are unoccupied), MnO (10% of the metal sites are unoccupied), NbN_{1-x} (23% of the nonmetal sites are unoccupied). The configurational entropy term makes a significant contribution to the stability of high-symmetry disordered structures leading to their stability at high temperatures, but with decreasing temperature

competing energetic factors lead to the formation of more ordered phases and narrower ranges of homogeneity through heterogeneous reaction. The stabilities of nonstoichiometric solids and the widths of their homogeneity ranges depend on the thermodynamic properties of both the defect phase and its adjacent phases.

Over extended ranges of composition the defect materials appear, in the absence of long-range order, monophasic in diffraction experiments. Often the symmetry of materials is lowered with decreasing temperature by ordering processes. Within the homogeneity range of the NaCl-type solids samples of all compositions can be described in terms of the common face-centered cubic unit-cell with the superposition of superstructure when the symmetry has been broken.[3] Usually the cell dimensions vary continuously with changing thermodynamic state through the symmetry change, which implies there is progressive and uniform change in structure. Such crystal structure changes may occur via one of the three types of transitions: order-disorder, displacive and combination of both.

The following is a brief review of the structure changes that have been found to occur in the homogeneity range of NaCl-type solids: a) In defect scandium-sulfur system, $Sc_{1-x}S$, the structure changes from cubic to rhombohedral with decreasing temperature. It was found that this transition corresponds to doubling of the periodicity along the body diagonal of the cubic cell (Fm3m space group) to yield $R\bar{3}m$ symmetry. The symmetry change was found to result from segregation of the scandium site vacancies into alternate (111) planes, and further ordering was observed within these planes using electron diffraction.[4] b)

Nonstoichiometric zirconium sulfides have been studied by number of groups since the earliest investigation in 1939.[5] F. Jellinek suggested that hyperstoichiometric ZrS has either a primitive cubic or a rhombohedral structure of $CdCl_2$-type.[6] Early work in Franzen's group yielded a monoclinic superstructure for $Zr_{.77}S$.[7,8] c) The crystal structure of Lu_3S_4 was solved and its orthorhombic structure described as a sheared population wave defect-ordering based on the NaCl-type lattice. In this system, the site occupation in metal containing planes varies periodically along the cubic (420) direction.[9] d) The nonstoichiometric mononitride of niobium, NbN_{1-x} has been studied a number of times. Brauer and Esselborn,[10] Guard and his coworkers,[11] and Christensen,[12] all present results that show a transition from cubic to tetragonal with decreasing temperature. However, the exact nature of the transition has not been completely clarified since x-ray, neutron and electron diffraction investigations as carried out by several groups led to contradictory results. e) Stoichiometric NbO and TiO also have ordered defect rock-salt type structures in which both metal and oxygen atoms are missing. In NbO, Nb and O are removed from the corners and the centers, respectively, of the face-centered cubic cell. The defect structure of TiO, in which 1/6 of the oxygen and metal atoms are missing, has been extensively studied by Watanabe.[13,14] f) In MnO and CoO, defects have been indicated and transitions from face-centered cubic to tetragonal and rhombohedral, respectively, were observed.[15]

The electronic transport properties of these compounds range from semiconductors to metallic conductors and even to low temperature superconductors. Many superconductors with what were, prior to recent

discoveries in the ternary copper oxides, relatively high superconducting transition temperatures have NaCl-type structure.[3,16,17] The superconducting properties of these solids change as a function of composition. Much work has been done on properties of superconducting nitrides, carbides and oxides.[18-23] As a notable example, for NbN_x it was found that T_c has a maximum at the 1:1 ideal metal-to-nonmetal ratio (T_c=18K).[24,25] Superconducting properties of $Zr_{1-x}S$, $Sc_{1-x}S$ and $Lu_{1-x}S$, as well as other selenides, sulfides and phosphides were reported by Moodenbaugh.[16]

The mechanisms of vacancy stabilization and ordering has attracted research interest. In many cases among oxides[26] and sulfides,[27] the ionic model fails to describe the stability of defect structures even though these compounds are quite polar.

Electronically driven mechanisms in TiO have been proposed by Huisman and coworkers,[28] Denker[29] and Goodenough.[30] After electronic structure calculation on one-to-one and an ordered defect ScS, Franzen and coworkers, following Huisman et al., proposed that the mechanism for vacancy stabilization is probably energetic, entropic stabilization being insufficient in cases with such large vacancy concentrations.[31] Burdett and Hughbanks[26] reported that the creation of vacancies enhances metal-metal bonding in the NbO and TiO systems to stabilize the unique crystal structures in the defect ordered materials.

One way to explain symmetry lowering deformations is via Peierls distortions. The partial filling of a band leads to an electron-phonon coupling which opens up a gap just at the Fermi level. In this way a continuous phase transition in a crystal can involve a soft mode. As

the lattice becomes unstable at certain temperatures, the mode corresponding to a given irreducible representation can become increasingly more active until a distortion results from a corresponding static displacement. The transition from NiAs to MnP structure in VS_x is an example of a displacive transition which was described by R. Hoffmann and W. Tremel[32,33] applying such arguments.

Although numerous efforts have been made to explain the nature of phase transitions in defect solids, not much is reliably known concerning these interesting phenomena.

The goal of this research is to examine the thermal behavior of NaCl-type defect solids to contribute to the understanding of the interrelationship between structure, stability and electronic structure in these materials. During the x-ray diffraction investigations the known NaCl-type diffraction patterns are changed because of line-splitting or the appearance of weak superstructure lines or both. It is difficult to determine an unknown distorted structure using only geometric considerations based on the NaCl-type sublattice. The space-group symmetry in this case (Fm3m) is a supergroup of all cubic space-group types, as well as all tetragonal, rhombohedral, orthorhombic and monoclinic space-group types. The problem is complicated because the nature of the formation process leads to multiple twinning and therefore good single crystals are not available in the low-symmetry compounds. There are far too many superstructure and distortion alternatives to permit the solution of structure using conventional x-ray powder diffraction alone. If there is no observation of two-phase coexistence, Landau theory of symmetry and phase transitions can be

applied to greatly reduce the number of solutions. The conditions for second-order phase transition from Landau theory provides remarkable guidelines for the solution of such problems. Finally these solutions can be used to refine the observed x-ray powder diffraction data using the full-profile refinement procedure.

In this study, the nature of order-disorder transitions in NbN_{1-x}, $Zr_{1-x}S$, $Lu_{1-x}S$ and $Y_{1-x}Se$ were investigated based on Landau theory of symmetry and phase transitions, and all the possible thermal symmetry breaking transitions are presented with examples where these have been observed.

LANDAU THEORY

Transitions between different crystal modifications usually take place via abrupt reconstruction of the crystal lattice, and the structure of a crystal undergoes a discontinuous change. However, besides such discontinuous transitions, another type of transition involving a change of symmetry is possible, namely one in which the arrangement of the atoms in a crystal changes continuously starting at a certain transition temperature. The transitions of the first kind are first-order phase transitions while those of the second kind are second-order. Such second-order transitions can occur via continuous displacement of atoms or via changes in ordering in the crystal or via a combination of both. An example of displacive transitions is the NiAs-type to MnP-type phase transition in which atomic positions change continuously away from high symmetry positions ($P6_3/mmc \rightarrow Pcmn$) with decreasing temperature.[34] The β-β' brass distortion[35] is the classical example of a pure order-disorder transition in which Zn and Cu atoms interchange their positions with increasing temperature. An example of the third type, the combination of displacive and order-disorder, is the NbN_{1-x} distortion which is discussed in this thesis.

In contrast to first-order transitions, second-order transitions occur without coexistence of two phases in equilibrium. At each temperature, even at the transition temperature, only one phase exists, so that such a transition is a transition within one phase not between two phases. At the transition point the solid acquires new symmetry properties without growth or nucleation of a new phase so that the

space-group symmetry of the crystal changes suddenly. This type of transition is only possible if certain conditions relating the symmetries above and below the transition point are fulfilled.

Both the theoretical and experimental understanding of the phase transitions under consideration have benefited greatly from the application of group-theoretical methods. Since Landau first applied this method for the case of continuous phase transitions, the validity of Landau's theory[36] has been demonstrated by its application to the intricate patterns of transitions observed in structural, magnetic and liquid crystalline transitions, and more recently, to the investigation of the properties of incommensurate phases.

Landau's[36-39] theory provides four conditions that a phase transition must meet in order that it be possible for the transition to occur continuously:

1) The space group of the two crystalline structures related by such a transition must be in a group-subgroup relationship.
2) The change of the crystal should correspond to a single irreducible representation of the space-group of higher symmetry.
3) There must be no third-order combination of the basis functions invariant under the symmetry operations of the group.
4) The space lattice of the lower symmetry structure must be locked in by symmetry.

In order to derive these symmetry conditions, Landau introduced the density function for the particles, ρ, and expressed the distorted

particle density, ρ, in terms of the undistorted particle density, ρ^o, and a combination of basis functions, $\Sigma_n \Sigma_i C_i{}^n \phi_i{}^n$, i.e.

$$\rho = \rho^o + \Sigma_n \Sigma_i C_i{}^n \phi_i{}^n$$

where linear combinations of the functions $\phi_i{}^n$ with a given n transform one into another under all transformations of the high-symmetry group, and n labels each irreducible representation. When the crystal changes continuously in such a way that the symmetry of the crystal is lowered, the new density function ρ can be written in terms of high symmetry density function ρ^o

$$\rho(r) = \rho^o(r) + \Delta\rho(r)$$

where $\Delta\rho$ is the term resulting from small change. Thus in the above $\Delta\rho(r)$ has been expanded in a complete set of basis functions of the group of ρ^o, as allowed by group theory. An arbitrarily small $\Delta\rho$ can destroy some of the symmetry operations of group of ρ^o, but cannot create new symmetry, and consequently the group of ρ is subgroup of the group of ρ^o. Furthermore, the symmetry group of ρ does not contain all of the elements contained in the high symmetry group of ρ^o. In general if one continuous transition occurs, the change corresponds to a single irreducible representation. Consequently the summation over n for different irreducible representations is omitted,

$$\rho(r) = \rho^o(r) + \Sigma_i C_i \phi_i$$

The changes of the crystal correspond to changes of the Gibbs free energy. The Gibbs free energy G of the crystal can be expressed as a function of intensive state and thus the coefficients C_i depend upon intensive state. The actual values of C_i as a function of P and T are determined by the equilibrium condition, i.e., G should be at a minimum. These coefficients also determine the symmetry of the low symmetry phase of the crystal since it is clear that symmetry of a function $\rho(r)$ is determined by the value of the coefficients of the linear combination of ϕ_i's.

For convenience the C_i's can be normalized after introducing the notation $\eta^2=\Sigma C_i^2$, the normalized coefficients, γ_i, are defined $C_i=\eta\gamma_i$, so that $\Sigma\gamma_i^2=1$. Since $\rho \rightarrow \rho^o$ as $C_i \rightarrow 0$, it is possible to expand G in a power series of in the C_i's (the product of η and γ_i) near the transition point:

$$G = G_o + \alpha\eta + A\eta^2 + B\eta^3 f^3(\gamma_i) + C\eta^4 f^4(\gamma_i) + \ldots$$

where, $f^n(\gamma_i)$ is a homogeneous function of order n in the γ_i's.

The free energy at $\eta = 0$ corresponds to a minimum for the stable symmetric phases, thus the linear term vanishes. In the presence of a third-degree term the value $\eta = 0$ does not correspond to minimum of free energy at the transition point, therefore a second-order phase transition is possible only if third order terms in free energy are zero, i.e., it is necessary that this term must vanish for symmetry reasons. The Gibbs free energy which is minimized to yield stable lower symmetry phases that result from second-order transitions is therefore:

$$G = G_0 + A\eta^2 + \eta^4 \Sigma_\alpha C_\alpha f_\alpha^4(\gamma_i),$$

where, because G is invariant under symmetry operations, the f^n's must be invariant combinations of the γ_i's and α labels independent invariants of corresponding order.

4th Condition

In reciprocal space the free energy G can be expanded in δk about a given k

$$G(k+\delta k)=G_0(k)+\alpha\cdot\delta k+\ldots$$

If there is a second-order phase transition at a wave-vector k with change of the structure corresponding to a particular irreducible representation, it is necessary that G has a minimum at the transition point. For G to have a minimum at a fixed k, the vector α must necessarily vanish at the k to which a second-order transition corresponds, i.e., there can be no vector invariant.

The fourth condition of Landau is met if the proper symmetry group of k contains inversion or intersecting axis and plane or an intersecting pair of axes. The k points obeying one of these conditions are the high symmetry points of the first Brillouin zone. (Even if this condition is not obeyed, a second-order phase transition is still

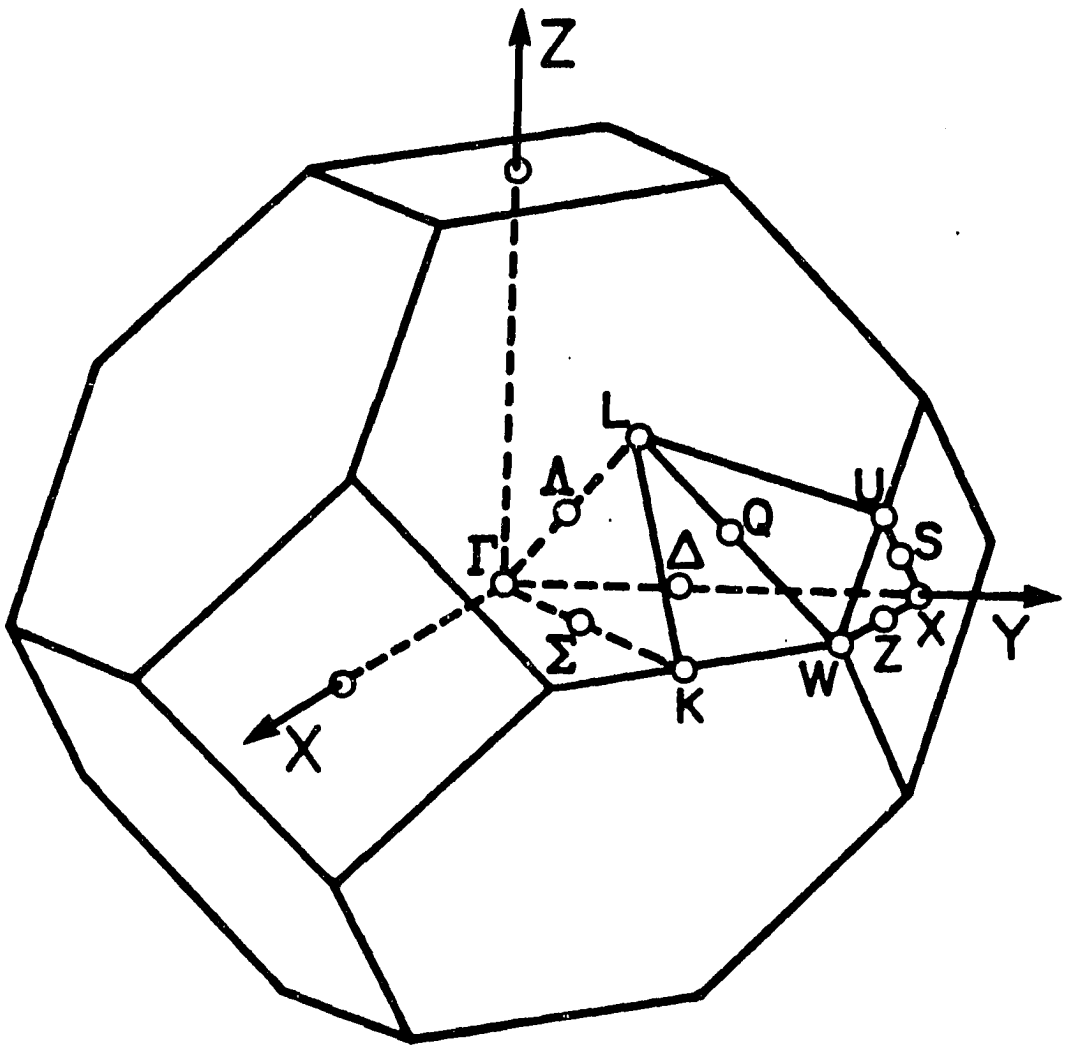

Figure 1. The body-centered cubic Brillouin zone with the high symmetry points indicated

possible, but then the low-symmetry structure cannot be described by an ordinary way. It is an incommensurate phase, a case that will not be considered here.)

For example, if the high-symmetry structure is NaCl-type, then such high symmetry points are: $\Gamma(k=0)$, $X(k=a^*,b^*,c^*)$, $W(k=\pm(a^*+c^*/2)$, $\pm(b^*+a^*/2)$, $\pm(c^*+b^*/2))$ and $L((k=a^*+b^*+c)/2$, $(a^*+b^*-c^*)/2$, $(a^*-b^*+c^*)/2$, $(-a^*+ b^*+c^*)/2)$.

An Example of a Transition at Special Point : L Point

It has been observed in metal deficient $Sc_{1-x}S$ and $Zr_{1-x}S$ that the vacancies, which are randomly distributed at high temperature, order in alternate 1,1,1 planes when the samples are cooled slowly.[3,40] The transition appears to occur continuously at the L point with four vectors in the star, i.e., k=(1/2,1/2,1/2), (-1/2,1/2,1/2), (1/2,-1/2,1/2), (1/2,1/2,-1/2). For example, if the transition corresponding to the single vector, $k=(a^*+b^*+c^*)/2$, is considered, then the translation operations $a_o+(b_o+c_o)/2$, $b_o+(a_o+c_o)/2$ and $c_o+(a_o+b_o)/2$ remain, whereas, those such as a_o and $(b_o+c_o)/2$ are lost (If T is translational symmetry operation of the parent cubic sublattice, then $k\cdot T$ is integral for all translations that remain). The result is a rhombohedral lattice with $a_{rh}=a_o+(b_o+c_o)/2$, $b_{rh}=b_o+(a_o+c_o)/2$ and $c_{rh}=c_o+(a_o+b_o)/2$. A basis function which is symmetric with respect to translations that remain and antisymmetric with respect to those that are lost can be found, e.g., $\cos(2\pi(a^*+b^*+c^*)/2\cdot r=\cos\pi(x+y+z)$. There

are then four basis functions which form a basis for an irreducible representation corresponding to the four vectors in the star:

$$\phi_1=\cos\pi(x+y+z)$$

$$\phi_2=\cos\pi(-x+y+z)$$

$$\phi_3=\cos\pi(x-y+z)$$

$$\phi_4=\cos\pi(x+y-z)$$

Evidently it is not possible to form third-order combinations from these basis functions and thus no third order invariant exist. These are basis functions corresponding to the totally symmetric small representation at the L point.

The Gibbs free energy of the ordered structure is expanded to fourth order in the coefficients of the ϕ_i's. The ϕ_i's form three independent fourth-order invariant combinations, i.e., $\Sigma\phi_i^4$, $\Sigma\phi_i^2\phi_j^2$, and $\phi_1\phi_2\phi_3\phi_4$. Thus $\Sigma\gamma_i^4$, $\Sigma\gamma_i^2\gamma_j^2$ and $\gamma_1\gamma_2\gamma_3\gamma_4$ are fourth-order invariant combinations of the γ_i's, but one of the three terms, $\Sigma\gamma_i^2\gamma_j^2$, can be eliminated by using $(\Sigma\gamma_i^2)^2=1$. Then the fourth-order term in G looks like

$$[C_1+C_2\Sigma\gamma_i^4+C_3\gamma_1\gamma_2\gamma_3\gamma_4]\eta^4$$

and the stable ordered structure will correspond to minima of this function subject to the restraint $\Sigma\gamma_i^2=1$. There are three types of solutions:

1) if $C_2 < C_3/12$, $\gamma_1=1$, $\gamma_2=\gamma_3=\gamma_4=0$

2) if $C_3 < 0$ and $C_2 > C_3/12$, $\gamma_1=\gamma_2=\gamma_3=\gamma_4=1/2$

3) if $C_3 > 0$ and $C_2 > C_3/12$, $\gamma_1=\gamma_2=\gamma_3=-\gamma_4=1/2$

These three solutions are the possible states of ordered structures arising from the NaCl-type structure at point L and corresponding to the totally symmetric small representation. The first solution yields a rhombohedral lattice and the other two solutions yield cubic lattices with doubled cell parameter.

The space groups corresponding to this (and other) irreducible representation at the L point can be determined by investigating the symmetries of these "stable" combinations of basis functions. The small representations show how the basis functions behave under the essential symmetry operations in the group of the wave vector.[41]

There are four 1-dimensional and two 2-dimensional small representations. The four 1-dimensional cases are shown in Table 1.

Table 1. The one-dimensional small representations for the L point

	E	$2C_3$	$3C_2$	i	$2S_3$	$3\sigma_d$
τ^1	1	1	1	1	1	1
τ^2	1	1	1	-1	-1	-1
τ^3	1	1	-1	1	1	-1
τ^4	1	1	-1	-1	-1	1

A transition corresponding to a small representation τ^1 corresponds to the totally symmetric representation, and the 12 essential symmetry operations listed in the table remain. It follows, as we have just seen, that the space group $R\bar{3}m$ results. But a transition corresponding to the representation τ^2 results in the loss of the essential i, S_3, σ_d operations of Fm3m. However, the product of these operations together with any lost translation is retained. For example σ_{y-x} ($=\sigma_d$) is lost, but σ_{y-x} followed by translation $a_o+b_o+c_o$ is not. The operation $\{\sigma_{y-x}|111\}$ implies a c-glide plane and the space group is $R\bar{3}c$. Similarly the representation τ^3 and τ^4 cases result in the $R\bar{3}c$ and $R\bar{3}m$ space groups, respectively.

Next it is necessary to determine the positions in those structures with $R\bar{3}m$ and $R\bar{3}c$ symmetry that are consistent with continuous change from NaCl-type symmetry. The two metal (0,0,0),(1/2,1/2,1/2) and two nonmetal (1/4,1/4,1/4), (3/4,3/4,3/4) positions are consistent with the NaCl-type structure. In $R\bar{3}m$ the (0,0,0) and (1/2,1/2,1/2) positions are decoupled, allowing for order-disorder, and the two nonmetal positions are coupled but variable, allowing for displacive distortion. However in $R\bar{3}c$ both positions are fixed and coupled allowing only for angle distortion of the lattice. The $R\bar{3}c$ case is thus a special case of the allowed $R\bar{3}m$ distortion.

The question remains, what cubic space groups result for solutions $\gamma_1=\gamma_2=\gamma_3=\gamma_4=1/2$ and $\gamma_1=\gamma_2=\gamma_3=-\gamma_4=1/2$. The space groups for each solution can be determined by examining how the combinations of basis functions transform. The two combination functions are

$$\psi_1=\cos\pi(x+y+z)+\cos\pi(-x+y+z)+\cos\pi(x-y+z)+\cos\pi(x+y-z)$$

and

$$\psi_2=-\cos\pi(x+y+z)+\cos\pi(-x+y+z)+\cos\pi(x-y+z)+\cos\pi(x+y-z).$$

The function ψ_1 transforms into itself under all symmetry operations of Fm3m and thus results in space group Fm3m. The second function transforms into itself under all operations that permute x, y, and z and under all operations that change three of the signs. All operations except those mentioned above are lost, but they can be recovered when they are combined with lost translation operations. For example, the operation σ_x is lost, but σ_x followed by (a+b)/2 is retained. It follows that the symmetry of the function ψ_2 is Fd3m.

There are two 2-dimensional small representations, E_g and E_u, at the L point as shown in Table 2.

For these 2-dimensional representations, the fourth condition must be tested first, by testing whether the antisymmetric square of the representation times the vector representation, V(g), contains the totally symmetric representation.[38] Since the character of antisymmetric square of representation equals $\{\chi^2(g)-\chi(g^2)\}$, the condition expressed by:

$$\Sigma_R\{\chi^2(g)-\chi(g^2)\}\cdot V(g)=0$$

where the g's are the elements of the point group of the wave vector and $\chi(g)$'s are the characters of the representation. This consideration is carried out for a two 2-dimensional representation as shown for the E_g representation in Table 3. The conclusion of this test is that the vector representation and the antisymmetric square of the small

Table 2. The two-dimensional representations for the L point

E_g : E	$C_3^2(x+y+z)$	$C_3(x+y+z)$	$C_2(y-x)$	$C_2(z-y)$	$C_2(z-x)$
$\begin{pmatrix} 1 & 0 \\ 0 & 1 \end{pmatrix}$	$\begin{pmatrix} \varepsilon^a & 0 \\ 0 & \varepsilon^2 \end{pmatrix}$	$\begin{pmatrix} \varepsilon^2 & 0 \\ 0 & \varepsilon \end{pmatrix}$	$\begin{pmatrix} 0 & 1 \\ 1 & 0 \end{pmatrix}$	$\begin{pmatrix} 0 & \varepsilon \\ \varepsilon^2 & 0 \end{pmatrix}$	$\begin{pmatrix} 0 & \varepsilon^2 \\ \varepsilon & 0 \end{pmatrix}$
i	S_3^2	S_3	$\sigma(y-x)$	$\sigma(z-y)$	$\sigma(z-x)$
$\begin{pmatrix} 1 & 0 \\ 0 & 1 \end{pmatrix}$	$\begin{pmatrix} \varepsilon & 0 \\ 0 & \varepsilon^2 \end{pmatrix}$	$\begin{pmatrix} \varepsilon^2 & 0 \\ 0 & \varepsilon \end{pmatrix}$	$\begin{pmatrix} 0 & 1 \\ 1 & 0 \end{pmatrix}$	$\begin{pmatrix} 0 & \varepsilon \\ \varepsilon^2 & 0 \end{pmatrix}$	$\begin{pmatrix} 0 & \varepsilon^2 \\ \varepsilon & 0 \end{pmatrix}$
E_u : $E_g \times \tau^2$					

$a_{\varepsilon=e^{\pi i/3}}$.

representation are orthogonal and therefore the product does not contain the totally symmetric representation of Fm3m.

As shown in Table 2, the representations are complex. For the physical applications considered here, the representation must be real. However, one can always construct a real representation from complex irreducible representations by combining complex-conjugate basis functions. For example, two complex-conjugate basis functions, ϕ_1 and ϕ_2, generate a complex irreducible representation, but combination of the basis functions: $\psi_1=1/\sqrt{2}(\phi_1+\phi_2)$, $\psi_2=1/i\sqrt{2}(\phi_1-\phi_2)$ transforms this complex representation into a real representation. Two complex basis functions which are found for this 2-dimensional small representation are

$$\phi_1=[\cos 2\pi(x+y-z)+\varepsilon\cos 2\pi(-x+y+z)+\varepsilon^2\cos 2\pi(x-y+z)]\cos\pi(x+y+z)$$

$$\phi_2=[\cos 2\pi(x+y-z)+\varepsilon\cos 2\pi(x-y+z)+\varepsilon^2\cos 2\pi(-x+y+z)]\cos\pi(x+y+z),$$

where $\varepsilon=e^{\pi i/3}$ and the combined two real basis functions are of the form:

Table 3. The application of fourth condition of Landau's theory

g	E	C_3^2	C_3	C_2	C_2'	C_2''	i	S_3^2	S_3	σ	σ'	σ''
g^2	E	C_3	C_3^2	E	E	E	E	S_3	S_3^2	E	E	E
$\chi(g)$	2	-1	-1	0	0	0	2	-1	-1	0	0	0
$\chi(g^2)$	2	-1	-1	2	2	2	2	-1	-1	2	2	2
$\chi^2(g)$	4	1	1	0	0	0	4	1	1	0	0	0
$\chi^2(g)-\chi(g^2)$	2	2	2	-2	-2	-2	2	2	2	-2	-2	-2
$V(g)$	3	0	0	-1	-1	-1	-3	0	0	1	1	1
$\Sigma\{\chi^2(g)-\chi(g^2)\}\cdot V(g)=$	6	0	0	2	2	2	-6	0	0	-2	-2	-2

$$\psi_1=[2\cos 2\pi(x+y-z)-\cos 2\pi(x-y+z)-\cos 2\pi(-x+y+z)]\cos\pi(x+y+z)$$

$$\psi_2=\sqrt{3}[\cos 2\pi(x-y+z)-\cos 2\pi(-x+y+z)]\cos\pi(x+y+z).$$

These basis functions correspond to the irreducible representation at $\mathbf{k}=(\mathbf{a}^*+\mathbf{b}^*+\mathbf{c}^*)/2$, and the other functions corresponding to the irreducible representation at the other wave vectors in the star are:

$\psi_3=\psi_1(-x, y, z)$ $\psi_5=\psi_1(x, -y, z)$ $\psi_7=\psi_1(x, y, -z)$

$\psi_4=\psi_2(-x, y, z)$ $\psi_6=\psi_2(x, -y, z)$ $\psi_8=\psi_2(x, y, -z)$

To find the stable structures corresponding to this 2-dimensional small representation, first consider the allowed fourth-order terms (which are combinations of the eight coefficients of ϕ_i's). There are two independent fourth-order terms, $\Sigma(\gamma_{2j+1}^2+\gamma_{2j+2}^2)^2$ and $(\Sigma\gamma_i^2)^2-\Sigma(\gamma_{2j+1}^2+\gamma_{2j+2}^2)^2$ for j=0,1,2,3, but the second term can be eliminated because $(\Sigma\gamma_i^2)^2=1$. Then the fourth-order term in G looks like

$$[C_1+C_2((\gamma_1^2+\gamma_2^2)^2+(\gamma_3^2+\gamma_4^2)^2+(\gamma_5^2+\gamma_6^2)^2+(\gamma_7^2+\gamma_8^2)^2)]\eta^4$$

The possible space lattices are found by minimizing this function with respect to the γ_i subject to the restraint $\Sigma\gamma_i^2=1$. There are two solutions; 1) if $C_2 < 0$ then $\gamma_{2j+1}^2+\gamma_{2j+2}^2=1$, for j=0,1,2,3 2) if $C_2 > 0$ then $\gamma_i=1/\sqrt{8}$ (i=1~8). From these two solutions the combinations of wave vectors to which possible superlattices correspond are found, and also the basis functions can be combined:

$$\Phi_1= \gamma_{2j+1}\psi_{2j+1} + \gamma_{2j+2}\psi_{2j+2} \quad \text{for } j=0,1,2,3$$
$$\Phi_2=(\psi_1+\psi_2+\psi_3+\psi_4+\psi_5+\psi_6+\psi_7+\psi_8)/\sqrt{8}$$

The allowed symmetries are determined by examining the symmetry of the basis functions. The space-group C2/m was found for both, but lattice dimensions are different in each case.

Similarly the other 2-dimensional representation, E_u, was examined and the real combinations of basis functions were found for the real irreducible representation corresponding to four k's in the star:

$\psi_1=[2\cos 2\pi(x+y-z)-\cos 2\pi(-x+y+z)-\cos 2\pi(x-y+z)]\cos\pi(x+y+z)(\sin 2\pi x-\sin 2\pi y)(\sin 2\pi y-\sin 2\pi z)(\sin 2\pi x-\sin 2\pi z)$,

$\psi_2=\sqrt{3}[\cos 2\pi(x-y+z)-\cos 2\pi(-x+y+z)]\cos\pi(x+y+z)(\sin 2\pi x-\sin 2\pi y)(\sin 2\pi y-\sin 2\pi z)(\sin 2\pi x-\sin 2\pi z)$;

$\psi_3=\psi_1(-x, y, z)$, $\psi_5=\psi_1(x, -y, z)$, $\psi_7=\psi_1(x, y, -z)$,

$\psi_4=\psi_2(-x, y, z)$, $\psi_6=\psi_2(x, -y, z)$, $\psi_8=\psi_2(x, y, -z)$.

The same two solutions minimize the fourth-order invariant function as in the E_g case. The allowed symmetries are C2/c for both solutions but with different lattice dimensions.

Excluding this example (the L-point), all the allowed structures arising continuously from NaCl-type based on the four conditions of Landau theory of symmetry and phase transitions are worked out in following chapter.

Application of Landau Theory for the Allowed Structure Arising Continuously from NaCl-type Structure : The Γ, X and W Points

In this chapter, the transitions corresponding to all high-symmetry points of the NaCl-type structure are considered. The procedure to find the low-symmetry structure followed in the preceding example is presented in detail below.

1. Determine the wave vectors in the star at each high-symmetry point in reciprocal space.
2. If the small representation is more than one-dimensional, the Landau fourth condition is tested to determine whether the

product of the vector representation and antisymmetric square of the representation contains the totally symmetric representation.[38]

3. Determine whether any third-order combination of the basis functions can be invariant with translational symmetry operations or essential symmetry operations.
4. If there is no third-order invariant combination of basis functions, then examine the fourth-order invariant combinations of the basis functions.
5. G is expressed with invariant coefficients of the basis functions (γ_i's) up to fourth-order and the solution which minimizes G with respect to the γ_i subject to the restraint $\Sigma\gamma_i^2=1$ is determined.
6. From the solutions in step 5, the combinations of the wave vectors and basis functions can be found. The space lattice and space group can be determined from the combinations of wave vectors and basis functions respectively.
7. Finally the atomic positions must be considered to determine whether positions in the structure are consistent with continuous change in phase to the NaCl-type.

The Transition Corresponding to Γ Point

If the transitions correspond to the wave vector k=0, i.e., if there is no superstructure, the small representations coincide with representations of the O_h point group.

In most cases, and it is true for k=0 of Fm3m, Landau's fourth-condition is satisfied for 2-dimensional and 3-dimensional small representations.[38] The character of the one-dimensinal irreducible representation of the translational subgroup, {T}, is $e^{-ik\cdot T}$ for translation T at given wave vector. For k=0 the density function $\delta\rho$ transforms into itself, i.e., $T\cdot\delta\rho=\delta\rho'=\Sigma e^{-k\cdot T}\eta_i\phi_i=\Sigma\eta_i\phi_i$ under the action of any translational symmetry T. Thus there exist third-order combinations of basis functions which are translationally invariant. The existence of such third-order combinations means that a second-order phase transition in Fm3m at the Γ point cannot correspond to the totally symmetric small representation. Thus among four 1-dimensional representations, A_{1g} is eliminated. The remainder of the representations A_{2g}, A_{1u} and A_{2u} result in Fm3, F43m and $F\bar{4}32$ symmetries, respectively. However, in all three of these space groups, the only possible nonmetal (0,0,0) and metal (1/2,1/2,1/2) positions are equivalent to those in Fm3m, and no distortion is possible. Thus there are no phase transitions corresponding to the 1-dimensional representations at k=0.

There are two 2-dimensional representations, E_g and E_u. The small representations are complex. Two complex basis functions corresponding to the E_g representation are

$$\phi_1=\varepsilon^2\cos 2\pi x+\varepsilon\cos 2\pi y+\cos 2\pi z$$

and

$$\phi_2=\varepsilon\cos 2\pi x+\varepsilon^2\cos 2\pi y+\cos 2\pi z.$$

The corresponding real representation can be generated from this complex irreducible representation by combining the two complex conjugate basis functions. The combined real basis functions are

$$\psi_1 = 2\cos 2\pi z - \cos 2\pi x - \cos 2\pi y$$

and

$$\psi_2 = \sqrt{3}(\cos 2\pi y - \cos 2\pi x).$$

To find stable structures corresponding to this 2-dimensional small representation, the invariant fourth-order terms in the Gibbs free energy expansion must be considered. In this case there is only one fourth-order invariant, $\gamma_1^4+\gamma_2^4+2\gamma_1^2\gamma_2^2$, therefore the stable solutions must be determined by consideration of the 6th order terms. However, since there are only two possible discrete solutions, ψ_1 and $\psi_1+\psi_2$, these are taken as the stable solutions. For later use note that the basis function ψ_1 has space-group symmetry I4/mmm, and the combination of basis function $\psi_1+\psi_2$ transforms into itself under the operations E, $3C_2$, 3σ and i, yielding space group Immm. However in the E_g case, the combination of basis function $\phi_1^3+\phi_2^3$ is invariant, which means that there are third-order combinations of real basis functions. Thus the transition corresponding to this case is eliminated.

In the E_u case, the two real basis functions are

$$\psi_1 = (2\cos 2\pi z - \cos 2\pi x - \cos 2\pi y)(\sin 2\pi x - \sin 2\pi y)(\sin 2\pi y - \sin 2\pi z)(\sin 2\pi z - \sin 2\pi x)$$

and

$$\psi_2=\sqrt{3}(\cos 2\pi y-\cos 2\pi x)(\sin 2\pi x-\sin 2\pi y)(\sin 2\pi y-\sin 2\pi z)(\sin 2\pi z-\sin 2\pi x).$$

The function ψ_1 has the space group I422 and the function $\psi_1+\psi_2$ corresponds to the space group I222. However, consideration of the atomic positions takes these two space groups back to the space groups I4/mmm and Immm which were found for the E_g case. Thus the transitions corresponding to the E_u representation are rejected for the same reason as in the E_g case.

Next, there are four 3-dimensional small representations, T_{1g}, T_{2g}, T_{1u} and T_{2u}. The allowed fourth-order terms are considered first. There are two independent invariant functions such as ϕ_k^4 and $\phi_i^2\phi_j^2$, because no symmetry operations transform ϕ_k^4 into $\phi_i^2\phi_j^2$, and thus the two fourth-order terms, $\Sigma\gamma_k^4$ and $\Sigma\gamma_i^2\gamma_j^2$, are independent fourth-order invariants in the Gibbs free energy expansion. One of the fourth-order terms can be eliminated by recalling that $\Sigma\gamma_i^2=1$, and thus $(\Sigma\gamma_i^2)^2=1$. The resulting fourth-order term in G looks like:

$$[C_1+C_2(\gamma_1^2\gamma_2^2+\gamma_2^2\gamma_3^2+\gamma_1^2\gamma_3^2)]\eta^4.$$

If $C_2 > 0$, then G can be minimized with $\gamma_i=1$ and $\gamma_i\neq\gamma_j=0$. For the other case, i.e., if $C_2 < 0$, $\gamma_1=\gamma_2=\gamma_3=1\sqrt{3}$ is a stable solution. Thus the functions ϕ_1 and $\phi_1+\phi_2+\phi_3$ are possible combinations of basis functions which have to be examined to find possible symmetries of the stable distorted structures.

In the T_{1g} case, the small representation[41] shows how the three basis functions transform under the 48 symmetry operation of point group

O_h. A single basis function, for example ϕ_1, transforms into itself under operations E, C_{2x}, $C_{2(z-y)}$, $C_{2(z+y)}$, i, σ_x, σ_{z-y} and σ_{z+y} to yield the previously eliminated space group Immm. The basis function $\phi_1+\phi_2+\phi_3$ transforms into itself under symmetry operations E, $C_3{}^2{}_{(x+y+z)}$, $C_{3(x+y+z)}$, $C_{2(y-x)}$, $C_{2(z-y)}$, $C_{2(z-x)}$, i, $i\cdot C_3{}^2{}_{(x+y+z)}$, $i\cdot C_3{}^2{}_{(x+y+z)}$, σ_{y-x}, σ_{z-y} and σ_{z-x} to yield space group $R\bar{3}m$. However in this case there exists a third-order invariant. For example the functions (ϕ_1, ϕ_2, ϕ_3) transform into (ϕ_2, $-\phi_3$, $-\phi_1$) under the symmetry operation $C_{3(x+y-z)}$ and etc. and thus the third-order combination $\phi_1\phi_2\phi_3$ transforms into itself. The transitions corresponding to T_{1g} are thus eliminated.

In the T_{2g} case, the basis function ϕ_1 transforms into itself under symmetry operations E, C_{2x}, $2C_{4x}$, i, σ_x, and $2S_{4x}$ to yield the space group I4/m. The basis function $\phi_1+\phi_2+\phi_3$ transforms into itself under symmetry operations E, $2C_3{}^2{}_{(x+y+z)}$, i and $2i\cdot C_3{}^2{}_{(x+y+z)}$ to yield space group $R\bar{3}$. However consideration of the possible atomic positions resulting from continuous distortion of the NaCl-type structure indicates that the resultant space groups are not I4/m and $R\bar{3}$, but rather are I4/mmm and $R\bar{3}m$ which were eliminated above. Thus there are no transitions corresponding to the T_{2g} representation.

Similarly for the T_{1u} case, the basis functions ϕ_1 and $\phi_1+\phi_2+\phi_3$ result in the space groups $I\bar{4}m2$ and R32 respectively, but with same reasoning as in T_{2g} case, those two space groups are eliminated.

Finally in the T_{2u} case, the basis function ϕ_1 transforms into itself under symmetry operations E, C_{2x}, $2C_{4x}$, σ_x, σ_y, σ_{z-y} and σ_{z+y} to yield the space group I4mm. The basis function $\phi_1+\phi_2+\phi_3$ transforms into

itself under symmetry operation E, $2C_{3(x+y+z)}$, σ_{y-x}, σ_{z-y} and σ_{z-x} to yield the space group R3m.

The Transitions Corresponding to X-Point

For the X-point there are three wave vectors in the star, ($\mathbf{k}=\mathbf{a}^*$, $\mathbf{b}^*$, $\mathbf{c}^*$), and these wave vectors can be combined to yield several space lattices. If the transitions correspond to a single wave vector, for example, $\mathbf{k}=\mathbf{c}^*$, then translations such as $(\mathbf{c}_o+\mathbf{a}_o)/2$ and $(\mathbf{c}_o+\mathbf{b}_o)/2$ are lost, whereas, those such as $(\mathbf{a}_o+\mathbf{b}_o)/2$ and $\mathbf{c}_o$ remain. A basis function which has the period $\mathbf{c}_o$ is found to be $\phi_3=\cos 2\pi z$, and $\phi_2=\cos 2\pi y$ and $\phi_1=\cos 2\pi x$ are the symmetrically equivalent basis functions with the periods $\mathbf{b}_o$ and $\mathbf{a}_o$ respectively.

However, a third-order combination of these basis functions that is invariant with respect to translation operations is found. While the third-order combination of basis functions $\phi_1^3+\phi_2^3+\phi_3^3$ transforms into $-\phi_1^3+\phi_2^3-\phi_3^3$ under the translational symmetry operation $(c^o+a^o)/2$ and thus is not invariant, another third-order combination of basis functions, $\phi_1\phi_2\phi_3$, transforms into itself under this and all other translational symmetry operations. Since the invariance under consideration includes invariance both with respect to translational symmetry operations and invariance with respect to the essential symmetry operations, the existence of this third-order term means that a second-order phase transition in Fm3m at the X-point cannot correspond to the totally symmetric small representation. For use later note that the totally symmetric 1-dimensional representation at the X-point would

yield the space group P4/mmm with $a_{tet} \simeq a_o/\sqrt{2}$, $c_{tet} \simeq a_o$, and this possibility is eliminated by the third condition of Landau.

Before consideration of the remaining 1-dimensional small representations, the possible combinations of wave vectors in the star are determined below. The dimension of an irreducible representation of a space-group is the product of the number of wave vectors in the star and the dimension of the small representation, thus the dimension of the irreducible representation corresponding to a 1-dimensional small representation at the X-point is three. As discussed above, the possible combinations of wave vectors in the star are determined by considering fourth-order invariant combinations of basis functions corresponding to an irreducible representation. In the case of the X point the fourth-order invariant term in G looks like:

$[C_1+C_2(\gamma_1^2\gamma_2^2+\gamma_2^2\gamma_3^2+\gamma_1^2\gamma_3^2)]\eta^4$, where $\Sigma\gamma_i^4$ has been eliminated using $(\Sigma\gamma_i^2)^2=1$.

The solutions minimizing G are of the two types, $\gamma_1=1$ and $\gamma_2=\gamma_3=0$ (if $C_2 > 0$), and $\gamma_1=\gamma_2=\gamma_3=1/\sqrt{3}$ (if $C_2 < 0$), showing that transitions corresponding to single wave vector or to all three wave vectors are the only possible cases.

The lattice that results from the first solution (the first solution corresponds to a single wave vector a^*) is a tetragonal lattice with $a_{tet}=(b_o+c_o)/2$, $c_{tet}=c_o$. The second solution corresponds to the set of three wave vectors a^*, b^*, c^*. If this set of all three vectors in the star at the X-point is considered, all the centering translations of the lattice appropriate to the NaCl-type are lost, but all translations

involving integral multiples of a_o, b_o and c_o remain, yielding a primitive cubic lattice with $a=a_o$.

There are eight 1-dimensional small representations which are the same as the representations of the D_{4h} point group, as shown in Table 4. All of the small representations are examined below except the totally symmetric small representation, A_{1g}, which was eliminated by the third condition of Landau.

Table 4. The one-dimensional small representations for the X-point

	E	$2C_4$	C_2	$2C_2'$	$2C_2''$	i	$2S_4$	σ_h	$2\sigma_v$	$2\sigma_d$
A_{1g}	1	1	1	1	1	1	1	1	1	1
A_{2g}	1	1	1	-1	-1	1	1	1	-1	-1
B_{1g}	1	-1	1	1	-1	1	-1	1	1	-1
B_{2g}	1	-1	1	-1	1	1	-1	1	-1	1
A_{1u}	1	1	1	1	1	-1	-1	-1	-1	-1
A_{2u}	1	1	1	-1	-1	-1	-1	-1	1	1
B_{1u}	1	-1	1	1	-1	-1	1	-1	-1	1
B_{2u}	1	-1	1	-1	1	-1	1	-1	1	-1

In the A_{2g} case, a transition corresponding to this small representation results in the loss of the symmetry operations $2C_2'$, $2C_2''$, $2\sigma_v$ and $2\sigma_d$ of Fm3m, however, the products of these operations together with lost translations are retained. For example, σ_x ($=\sigma_v$) is lost, but σ_x followed by translation $(a_o+c_o)/2$ is not, and σ_{x+y} (σ_d) is

lost, but σ_{x+y} followed by translation $(a_o+c_o)/2$ is not. Since the symmetry operations $(\sigma_z|0\ 0\ 0)$, $(\sigma_x|1/2\ 0\ 1/2)$ and $(\sigma_{x+y}|1/2\ 0\ 1/2)$ in the original cubic system are $(\sigma_z|0\ 0\ 0)$, $(\sigma_{x+y}|0\ 0\ 1/2)$ and $(\sigma_x|0\ 1/2\ 1/2)$, respectively, in the tetragonal system, the resultant space group is P4/mnc.

In this space group two metal (0,0,0, and 1/2,1/2,1/2) and two nonmetal (0,0,1/2 and 1/2,1/2,0) positions are consistent with the NaCl-type structure. In P4/mmm these two metal (0,0,0) and (1/2,1/2,1/2) positions are decoupled as are the two nonmetal (0,0,1/2) and (1/2,1/2,0) positions, allowing an order-disorder transition in addition to tetragonal distortion of the lattice, thus transition to P4/mnc is a more restrictive special case of the transition to P4/mmm. However, the P4/mmm case was eliminated because of a third-order invariant, thus the possibility of continuous transition to P4/mnc is also eliminated.

In the B_{1g} case, the basis function transforms into itself with respect to E, C_2, $2C_2'$, i, σ_h and $2\sigma_v$, and transforms into itself with respect to $2C_4$, $2C_2''$, $2S_4$ and $2\sigma_d$ only when these operations are combined with a lost translation such as $(a^o+c^o)/2$. When the symmetry operations, C_{4z} $(=C_4)$ and σ_{y+x} $(=\sigma_d)$ are combined with translational symmetry $(a^o+c^o)/2$, these two operations make a screw operation and a glide operation, respectively. Since $(\sigma_{y+x}|1/2\ 0\ 1/2)$ in the original cubic system is $(\sigma_x|1/2\ 1/2\ 1/2)$, an n glide, in the tetragonal system, the space group is $P4_2/mnm$. However, by the consideration of atomic positions, this symmetry is eliminated by the same reasoning as in the A_{2g} case.

Similarly in the B_{2g}, B_{1u} and B_{2u} cases, the space groups yield $P4_2/mmc$, $P4_2/nmc$ and $P4_2/nnm$ respectively. However, consideration of the atomic positions indicates that those are all special cases of the unallowed transition to P4/mmm, thus the transitions corresponding to these representations are eliminated as continuous processes.

In the A_{1u} case, the combinations of essential symmetry operations i, $2S_4$, σ_h (σ_z), $2\sigma_v$ (σ_x, σ_y), and $2\sigma_d$ (σ_{x+y}, σ_{x-y}) with a translational operation such as $(a_o+c_o)/2$ remain. The symmetry operations ($\sigma_z|1/2\ 0\ 1/2$), ($\sigma_x|1/2\ 0\ 1/2$) and ($\sigma_{x+y}|1/2\ 0\ 1/2$) in the original cubic system are ($\sigma_z|1/2\ 1/2\ 0$), ($\sigma_{x+y}|0\ 0\ 1/2$) and ($\sigma_x|0\ 1/2\ 1/2$) in tetragonal system. Thus, the space group is P4/nnc.

However, the two metal (0,0,0 and 1/2,1/2,1/2) and nonmetal (0,0,1/2 and 1/2,1/2,0) positions in the tetragonal lattice are equivalent in this space group and the resultant structure is same as the I4/mmm solution at the Γ point. Thus this small representation is eliminated.

In the A_{2u} case, the symmetry operation σ_h ($=\sigma_z$) is lost, however, the product of this operation together with a lost translation, $(a_o+c_o)/2$ or $(b_o+c_o)/2$, is retained. The symmetry operation ($\sigma_z|1/2\ 0\ 1/2$) in the cubic structure is ($\sigma_z|1/2\ 1/2\ 1/2$) in the new tetragonal lattice, and this operation indicates an n glide. Thus, the space group is P4/nmm. In this space group the positions $\pm(1/4, 1/4, z)$ with $z\simeq1/4$ for the metal atoms and $z\simeq3/4$ for nonmetal atoms are consistent with continuous transition to the NaCl-type structure.

Since the combination of basis functions $\phi_1\phi_2\phi_3$ is invariant with respect to translational symmetry operations, it is necessary that this third-order product not be invariant with respect to the essential

symmetry operations if transition to P4/nmm is to occur continuously. The A_{2u} small representation implies that the basis functions (ϕ_1, ϕ_2, ϕ_3) transform into ($-\phi_1$, $-\phi_2$, $-\phi_3$) with respect to inversion through the origin, and thus $\phi_1\phi_2\phi_3$ transforms into $-\phi_1\phi_2\phi_3$, and no third-order invariant combination of basis functions exists. Thus, a second-order phase transition to a tetragonal structure with P4/nmm symmetry is possible from NaCl-type structure.

The question remains, what primitive cubic space group results for the $\gamma_1=\gamma_2=\gamma_3=1/\sqrt{3}$ solution with $a=a_o$. To answer this question, it is useful to examine basis functions that transform as the small A_{2u} representation and as the translational symmetry of the P4/nmm solution. Noting that the basis function corresponding to c^* is antisymmetric with respect to z and symmetric with respect to x and y, and that the function has the period c_o in the c direction, $\phi_1=\sin 2\pi z$ is found to be a proper basis function, and $\phi_2=\sin 2\pi x$ and $\phi_3=\sin 2\pi y$ are basis functions with the periods a_o and b_o respectively. Thus the cubic space group has the symmetry of $\psi=\sin 2\pi x+\sin 2\pi y+\sin 2\pi z$. This basis function transforms into itself under all operations that permute x, y, and z and under all operations that change an even number of signs when combined with one of the centering translations of Fm3m. For example, C_{2x} transforms (x, y, z) into (x, $\bar{y}$, $\bar{z}$) and ψ is not invariant under C_{2x}. However, C_{2x} followed by $(b_o+c_o)/2$ takes ψ into itself and is preserved in the lower symmetry cubic group. On the other hand, all symmetry operations that change an odd number of signs (C_4, i, σ_x, σ_y and σ_z) are lost, and cannot be recovered by tacking on a lost translation. It follows that the space group of ψ is $P\bar{4}3m$.

There are two 2-dimensional small representations at X point, E_g and E_u, as shown in Table 5.

Table 5. Two-dimensional small representations for the X-point

E	C_{4z}	C_{2z}	C_{4z}^3	C_{2x}	$C_{2(y-x)}$	C_{2y}	$C_{2(x+y)}$
$\begin{pmatrix} 1 & 0 \\ 0 & 1 \end{pmatrix}$	$\begin{pmatrix} i & 0 \\ 0 & -i \end{pmatrix}$	$\begin{pmatrix} -1 & 0 \\ 0 & -1 \end{pmatrix}$	$\begin{pmatrix} -i & 0 \\ 0 & i \end{pmatrix}$	$\begin{pmatrix} 0 & 1 \\ 1 & 0 \end{pmatrix}$	$\begin{pmatrix} 0 & -i \\ i & 0 \end{pmatrix}$	$\begin{pmatrix} 0 & -1 \\ -1 & 0 \end{pmatrix}$	$\begin{pmatrix} 0 & i \\ -i & 0 \end{pmatrix}$
i	S_{4z}^3	σ_z	S_{4z}	σ_x	σ_{y-x}	σ_y	σ_{x+y}
$\begin{pmatrix} 1 & 0 \\ 0 & 1 \end{pmatrix}$	$\begin{pmatrix} i & 0 \\ 0 & -i \end{pmatrix}$	$\begin{pmatrix} -1 & 0 \\ 0 & -1 \end{pmatrix}$	$\begin{pmatrix} -i & 0 \\ 0 & i \end{pmatrix}$	$\begin{pmatrix} 0 & 1 \\ 1 & 0 \end{pmatrix}$	$\begin{pmatrix} 0 & -i \\ i & 0 \end{pmatrix}$	$\begin{pmatrix} 0 & -1 \\ -1 & 0 \end{pmatrix}$	$\begin{pmatrix} 0 & i \\ -i & 0 \end{pmatrix}$

and $E_u = E_g \times A_{1u}$.

Landau's fourth-condition was tested and it was concluded that the vector representation and antisymmetric square of the small representation are orthogonal for the E_g and E_u representations, and hence the fourth condition is met by the 2-dimensional small representations at the X-point.

As shown in Table 5, the small representations are complex. If the transition corresponds to a single wave vector $\mathbf{k}=\mathbf{c}^*$, the basis functions are antisymmetric with respect to the translational symmetry operations, $(b_o+c_o)/2$ and $(a_o+c_o)/2$, and symmetric with respect to $(a_o+b_o)/2$. Two basis functions which transform as the small representation of Table 5, and have the correct translational symmetry operations are found to be:

$$\phi_1=(\sin 2\pi x \cos 2\pi y + i \sin 2\pi y \cos 2\pi x)\cos 2\pi z \sin 2\pi z$$

and

$$\phi_2=(\sin 2\pi x\cos 2\pi y-i\sin 2\pi y\cos 2\pi x)\cos 2\pi z\sin 2\pi z.$$

The combined two real basis functions are of the form:

$$\psi_1=\sin 2\pi x\cos 2\pi y\cos 2\pi z\sin 2\pi z$$

and

$$\psi_2=\sin 2\pi y\cos 2\pi x\cos 2\pi z\sin 2\pi z.$$

The allowed symmetries of the low-symmetry structure can be determined by examining these two basis functions. The single basis function ψ_1 transforms into itself under the operations E, C_{2y}, i and σ_y, and also under the operations C_{2z}, C_{2x}, σ_z and σ_x when those operations are combined with a lost translation (e.g. $(a_o+c_o)/2$). The resultant space group is Pnnm, and the only positions allowed by the requirement of continuous transition to NaCl-type structure are the fixed 2-fold positions that form a body-centered cell. This means that the symmetry and continuity requirements are met only by a distortion that is equivalent to one at the Γ point and has been shown to yield a third-order invariant.

In the E_u case, the real basis functions which are formed from complex conjugate basis functions with the period corresponding to $k=c^*$ are:

$$\psi_1=\cos 2\pi y\sin 2\pi y\cos 2\pi z(\cos 4\pi x-\cos 4\pi y)$$

and $$\psi_2=\cos 2\pi x\sin 2\pi x\cos 2\pi z(\cos 4\pi y-\cos 4\pi x),$$

and considering the remaining k vectors in the star, a^* and b^*, adds the basis functions

$$\psi_3=\cos 2\pi x \sin 2\pi x \cos 2\pi y(\cos 4\pi z-\cos 4\pi x),$$

$$\psi_4=\cos 2\pi z \sin 2\pi z \cos 2\pi y(\cos 4\pi x-\cos 4\pi z),$$

$$\psi_5=\cos 2\pi z \sin 2\pi z \cos 2\pi x(\cos 4\pi y-\cos 4\pi z),$$

and $$\psi_6=\cos 2\pi y \sin 2\pi y \cos 2\pi x(\cos 4\pi z-\cos 4\pi y).$$

To carry on with a Landau theory analysis it is necessary to consider the existence of third-order, and the nature of fourth-order, invariant combinations of these basis functions. Since the functions (ψ_1,ψ_2) transform into $(-\psi_1, -\psi_2)$ under inversion through the origin, and thus ψ_1^3 transforms into $-\psi_1^3$, it follows that a second-order phase transition corresponding to the E_u small representation at the X-point is allowed by Landau theory.

As regards fourth-order invariants, considering how the functions behave under the symmetry operation of O_h yields five fourth-order invariants,

1. $\psi_1^4+\psi_2^4+\psi_3^4+\psi_4^4+\psi_5^4+\psi_6^4$
2. $\psi_1^2\psi_2^2+\psi_3^2\psi_4^2+\psi_5^2\psi_6^2$
3. $\psi_1^2\psi_3^2+\psi_3^2\psi_5^2+\psi_1^2\psi_5^2+\psi_2^2\psi_4^2+\psi_4^2\psi_6^2+\psi_2^2\psi_6^2$
4. $\psi_1^2\psi_4^2+\psi_3^2\psi_6^2+\psi_2^2\psi_5^2$
5. $\psi_1^2\psi_6^2+\psi_2^2\psi_3^2+\psi_4^2\psi_6^2$.

It follows that G, to fourth-order, is of the form

$$G = G_o + A\eta^2 + [C_1+(\gamma_1^2\gamma_2^2+\gamma_3^2\gamma_4^2+\gamma_5^2\gamma_6^2)C_2 + (\gamma_1^2\gamma_3^2+\gamma_3^2\gamma_5^2+\gamma_1^2\gamma_5^2+\gamma_2^2\gamma_4^2+\gamma_4^2\gamma_6^2+\gamma_2^2\gamma_6^2)C_3 + (\gamma_1^2\gamma_4^2+\gamma_3^2\gamma_6^2+\gamma_2^2\gamma_5^2)C_4 + (\gamma_1^2\gamma_6^2+\gamma_2^2\gamma_3^2+\gamma_4^2\gamma_5^2)C_5]\eta^4$$

and, because $\Sigma\gamma_i^2=1$, and therefore $(\Sigma\gamma_i^2)^2 = \Sigma\gamma_i^4 + 2\Sigma_{i\neq j}\gamma_i^2\gamma_j^2=1$, $\Sigma\gamma_i^4$ is eliminated in favor of $\Sigma_{i\neq j}\gamma_i^2\gamma_j^2$.

The minima of G subject to the normalization restraint $\Sigma\gamma_i^2=1$ are found by Legrange's method using λ as the undetermined multiplier when

$$\begin{aligned}
&\lambda\gamma_1 + C_2\gamma_1\gamma_2^2 + C_3\gamma_1(\gamma_3^2 + \gamma_5^2) + C_4\gamma_1\gamma_4^2 + C_5\gamma_1\gamma_6^2 = 0,\\
&\lambda\gamma_2 + C_2\gamma_2\gamma_1^2 + C_3\gamma_2(\gamma_4^2 + \gamma_6^2) + C_4\gamma_2\gamma_5^2 + C_5\gamma_2\gamma_3^2 = 0,\\
&\lambda\gamma_3 + C_2\gamma_3\gamma_4^2 + C_3\gamma_3(\gamma_1^2 + \gamma_5^2) + C_4\gamma_3\gamma_6^2 + C_5\gamma_3\gamma_2^2 = 0,\\
&\lambda\gamma_4 + C_2\gamma_4\gamma_3^2 + C_3\gamma_4(\gamma_2^2 + \gamma_6^2) + C_4\gamma_4\gamma_1^2 + C_5\gamma_4\gamma_5^2 = 0,\\
&\lambda\gamma_5 + C_2\gamma_5\gamma_6^2 + C_3\gamma_5(\gamma_1^2 + \gamma_3^2) + C_4\gamma_5\gamma_2^2 + C_5\gamma_5\gamma_4^2 = 0,\\
&\lambda\gamma_6 + C_2\gamma_6\gamma_5^2 + C_3\gamma_6(\gamma_2^2 + \gamma_4^2) + C_4\gamma_6\gamma_3^2 + C_5\gamma_6\gamma_1^2 = 0,\\
&\gamma_1^2 + \gamma_2^2 + \gamma_3^2 + \gamma_4^2 + \gamma_5^2 + \gamma_6^2 = 1.
\end{aligned}$$

These equations have been solved for the cases 1) all $\gamma_i \neq 0$, 2) three $\gamma_i \neq 0$, 3) two $\gamma_i \neq 0$ and 4) one $\gamma_i=1$. Two types of solutions result, "discrete" solutions for which the nonzero γ_i are equal in magnitude and continuous solutions for which they are not.

The discrete solutions found for minima in G together with sufficient conditions relating the C_i's to yield the minima are listed below.

I. $\gamma_1=1$, $\gamma_{i\neq1}=0$; $C_1 < 0$, $C_{i\neq1} > 0$

II. $\gamma_1=\gamma_2=1/\sqrt{2}$, $\gamma_{i>2}=0$; $C_2 < 0$, $C_{i\neq 2} > 0$

III. $\gamma_1=\gamma_4=1/\sqrt{2}$, $\gamma_2=\gamma_3=\gamma_5=\gamma_6=0$; $C_4 < 0$, $C_{i\neq 4} > 0$

IV. $\gamma_1=\gamma_6=1/\sqrt{2}$, $\gamma_2=\gamma_3=\gamma_4=\gamma_5=0$; $C_5 < 0$, $C_{i\neq 5} > 0$

V. $\gamma_1=\gamma_3=\gamma_5=1/\sqrt{3}$, $\gamma_2=\gamma_4=\gamma_6=0$; $C_3 < 0$, $C_{i\neq 3} > 0$

VI. $\gamma_i=1\sqrt{6}$; $(C_2+2C_3+C_4+C_5)/12 < C_2/4$, $C_4/4$, $C_5/4$ and $C_3/3$.

The first solution results in the transition corresponding to a single wave vector $k=c^*$, and the allowed symmetries of the low-symmetry structure can be determined by examining the single basis function ψ_1. The basis function ψ_1 transforms into itself under the operations E, C_{2z}, C_{2x}, i and σ_y when these operations are combined with a lost translation such as $(b_o+c_o)/2$. The resultant space group is Cmcm with $a\simeq b\simeq c\simeq a_o$.

The second solution yields the primitive orthorhombic cell with $a\simeq c\simeq a_o/\sqrt{2}$, $b\simeq a_o$, and the combination of basis functions $\psi_1+\psi_2$ has Pnmm symmetry.

The remaining discrete solutions correspond to sets of wave vectors that imply loss of all centering translations of the original Fm3m space group. The solutions labeled III, IV, V and VI yield the space groups P4/nmm, $P4_2/mnm$, $P2_13$ and R32, respectively, with $a\simeq b\simeq c\simeq a^o$ in all cases.

However, an unusual feature of the solution to the minimization of G in the case under discussion is the existence of a continuum of minimum solutions between these discrete solutions. For example, the continuum solution between the $\gamma_1=\gamma_2=1/\sqrt{2}$ and the $\gamma_1=\gamma_4=1/\sqrt{2}$ is $\gamma_1\neq\gamma_2\neq\gamma_4\neq 0$, $\gamma_3=\gamma_5=\gamma_6=0$, where γ_1, γ_2 and γ_4 generally differ in magnitude. Such a typical continuous solution is given below:

$$\gamma_1^2 = (C_2C_3+C_3C_4-C_3^2)/(2(C_2C_3+C_3C_4+C_2C_4)-C_2^2-C_3^2-C_4^2),$$
$$\gamma_2^2 = (C_2C_4+C_3C_4-C_4^2)/(2(C_2C_3+C_3C_4+C_2C_4)-C_2^2-C_3^2-C_4^2),$$
$$\gamma_4^2 = (C_2C_3+C_2C_4-C_2^2)/(2(C_2C_3+C_3C_4+C_2C_4)-C_2^2-C_3^2-C_4^2),$$

where γ_i's are functions of state because the C_i's are. For some choice of C_i's these γ_i's yield a G lower than for any discrete solution, and thus these continuous solutions can yield minima as well, perhaps, as saddle points. For the case of negative C_2, C_3, C_4 and positive C_5, if C_2 is sufficiently negative then the stable solution is the discrete solution $\gamma_1=\gamma_2=1/\sqrt{2}$ and the symmetry is Pnmm, but if C_4 is sufficiently negative then $\gamma_1=\gamma_4=1/\sqrt{2}$ is the stable solution with the symmetry $P4_2/mnm$, and if $C_3 < 3/4C_4$ or $C_3 < 3/4C_2$, then the stable solution is $\gamma_1=\gamma_3=\gamma_5=1/\sqrt{3}$ and the symmetry is $P2_13$. The boundary lines between these solutions and the continuum solutions, which are seen by the symmetry of an arbitrary mixture of ψ_1, ψ_2 and ψ_4 to have space group symmetry $P2_1/c$ with $a\simeq a_o$, $b\simeq a_o$, $c\simeq a_o$ and $\gamma\simeq 90°$, are given by $C_4-C_2=C_3$ and $C_2-C_4=C_3$.

There are similar continuum solutions for the region between the discrete Pnmm solution and the discrete P4/nmm solution ($P2_1/m$ with $a\simeq b\simeq c\simeq a_o$), and for the region between the $P4_2/mnm$ solution and the P4/nmm solution ($Pmn2_1$ with $a\simeq b\simeq c\simeq a_o$). The solutions can be characterized in terms of the basis functions as follows:

$1/\sqrt{2}(\psi_1+\psi_2)$: Pnmm discrete solution

$\gamma_1\psi_1+\gamma_2\psi_2+\gamma_4\psi_4$: $P2_1/c$ continuous solution

$1/\sqrt{2}\ (\psi_1+\psi_4)$: $P4_2/mnm$ discrete solution

$\gamma_1\psi_1+\gamma_4\psi_4+\gamma_6\psi_6$: $Pmn2_1$ continuous solution

$1/\sqrt{2}(\psi_1+\psi_6)$: $P4/nmm$ discrete solution

$\gamma_1\psi_1+\gamma_2\psi_2+\gamma_6\psi_6$: $P2_1/m$ continuous solution.

The Transition Corresponding to W-Point

For the W-point there are six wave vectors in the star: $\mathbf{k}=\pm(\mathbf{a}^*+\mathbf{c}^*/2)$, $\pm(\mathbf{b}^*+\mathbf{a}^*/2)$ and $\pm(\mathbf{c}^*+\mathbf{b}^*/2)$. There are only three equivalent body-centered tetragonal space lattices implied by these six wave vectors. For example, $\mathbf{k}=\mathbf{a}^*+\mathbf{c}^*/2$ and $-\mathbf{a}^*-\mathbf{c}^*/2$ are not equivalent in reciprocal space, but yield the same period.

If the transition corresponds to either the wave vector $\mathbf{k}=\mathbf{a}^*+\mathbf{c}^*/2$ or $-\mathbf{a}^*-\mathbf{c}^*/2$, all of the centering translations of Fm3m are lost, but translations $1/2\mathbf{a}_o+1/2\mathbf{b}_o+\mathbf{c}_o$, $\mathbf{b}_o$ and $\mathbf{a}_o$ remain, and yield a body-centered tetragonal cell with $c\simeq 2a_o$ and $a\simeq a_o$.

There are four 1-dimensional and one 2-dimensional small representations for the W-point as shown in Table 6.

First, the 1-dimensional small representations (which coincide with representations of the D_{2d} point group) are considered. The basis functions for each of the representations have translation symmetry correspond to $\mathbf{k}$ and transform according to the small representations. The basis functions which have this translational symmetry and are symmetric with respect to all of the operations in the group of wave vectors $\mathbf{k}=\mathbf{a}^*+1/2\mathbf{c}^*$ and $-\mathbf{a}^*-1/2\mathbf{c}^*$ are

$\phi_1 = e^{\pi i}\cos 2\pi x + e^{-\pi i}\cos 2\pi y,$

and $\phi_2 = e^{-\pi i}\cos 2\pi x + e^{\pi i}\cos 2\pi y$, respectively. They are complex.

Table 6. The small representations for the W-point

	E	S_{4z}^3	C_{2z}	S_{4z}	σ_y	$C_{2(y+x)}$	σ_x	$C_{2(y-x)}$
A_1	1	1	1	1	1	1	1	1
A_2	1	1	1	1	-1	-1	-1	-1
B_1	1	-1	1	-1	-1	1	-1	1
B_2	1	-1	1	-1	1	-1	1	-1
E	$\begin{pmatrix} 1 & 0 \\ 0 & 1 \end{pmatrix}$	$\begin{pmatrix} i & 0 \\ 0 & -i \end{pmatrix}$	$\begin{pmatrix} -1 & 0 \\ 0 & -1 \end{pmatrix}$	$\begin{pmatrix} -i & 0 \\ 0 & i \end{pmatrix}$	$\begin{pmatrix} 0 & 1 \\ 1 & 0 \end{pmatrix}$	$\begin{pmatrix} 0 & -i \\ i & 0 \end{pmatrix}$	$\begin{pmatrix} 0 & -1 \\ -1 & 0 \end{pmatrix}$	$\begin{pmatrix} 0 & i \\ -i & 0 \end{pmatrix}$

Since the basis functions corresponding to a distortion must be real, the two real basis functions are generated by combining the complex basis functions:

$$\psi_1 = 1/\sqrt{2}(\phi_1+\phi_2) = \cos\pi z(\cos 2\pi x+\cos 2\pi y)$$
$$\psi_1' = 1/\sqrt{2}i(\phi_1-\phi_2) = \sin\pi z(\cos 2\pi x+\cos 2\pi y).$$

Since the wave vectors **k** and **-k** yield the same period, and are related by a center of symmetry, the combinations of basis functions corresponding to such a pair of wave vectors have inversion symmetry in

addition to the D_{2d} point group symmetry. The first basis function ψ_1 is totally symmetric with respect to the symmetry operations of D_{2d} and to inversion as well, it thus yields the space group I4/mmm. The symmetry of the second basis function ψ_1' is also I4/mmm but, with a different origin. Since the pairs of basis functions have the same period and symmetry, this 6-dimensional irreducible representation can be treated as a 3-dimensional irreducible representation by choosing one basis function out of each pair.

Next, in the A_2 case, the basis function is antisymmetric with respect to σ_y and σ_x, but symmetric with respect to such operations together with the translational operation c_0. The space group is I4/mcm. The other two representations B_1 and B_2 yield I4/mcm and I4/mmm, respectively.

In the space group I4/mmm, two 4-fold metal (0, 0, z) with z≈1/4, and (0, 1/2, 0) positions, and two 2-fold nonmetal (0, 0, 0), (0, 0, 1/2), and a 4-fold nonmetal (0, 1/2, 1/4) position allow a combined order-disorder and displacive distortion. However, in the space group I4/mcm, two 4-fold metal (0, 0, 1/4) and (0, 1/2, 0) positions are fixed, and two 4-fold nonmetal (0, 0, 0) and (0, 1/2, 1/4) positions only allow the order-disorder transition.

The totally symmetric real basis function corresponding to $\mathbf{k}=\pm(\mathbf{a}^*+1/2\mathbf{c}^*)$ was given above: $\psi_1=\psi(x, y, z)=\cos\pi z(\cos 2\pi x+\cos 2\pi y)$. The complete irreducible real representation is generated by the basis functions $\psi_1=\psi(x, y, z)$, $\psi_2=\psi(y, z, x)$ and $\psi_3=\psi(z, x, y)$.

The fourth-order term in G to be minimized is

$$[C_1+C_2(\gamma_1^2\gamma_2^2+\gamma_2^2\gamma_3^2+\gamma_1^2\gamma_3^2)]\eta^4$$

This function exhibits two possible minima subject to $\Sigma\gamma_i^2=1$: $\gamma_1=1$, $\gamma_2=\gamma_3=0$ when $C_2 < 0$ and $\gamma_1=\gamma_2=\gamma_3=1/\sqrt{3}$ when $C_2 > 0$.

The former solution is the I4/mmm solution discussed above. The latter is a solution with the symmetry $\psi_1+\psi_2+\psi_3$. This function has the translational symmetry of a cubic lattice with $a\simeq 2a_o$ and space group symmetry Pm3m. Similarly a cubic solution with $a\simeq 2a_o$ corresponding to the the I4/mcm solution results when $\gamma_1=\gamma_2=\gamma_3=1/\sqrt{3}$.

For the 2-dimensional small representation $\psi_1=\psi(z, x)=\cos\pi z\sin 2\pi x$ and $\psi_2=\psi(z, y)$ form a basis. The complete 6-dimensional irreducible representation is generated by the basis set $\psi_1=\psi(z, x)$, $\psi_2=\psi(z, y)$, $\psi_3=\psi(x, y)$, $\psi_4=\psi(x, z)$, $\psi_5=\psi(y, z)$ and $\psi_6=\psi(y, z)$.

These functions permute under the symmetry operations such that the invariant fourth-order combinations of basis functions are:

$$\psi_1^2\psi_2^2+\psi_3^2\psi_4^2+\psi_5^2\psi_6^2$$
$$\psi_1^2\psi_3^2+\psi_3^2\psi_5^2+\psi_1^2\psi_5^2+\psi_2^2\psi_4^2+\psi_4^2\psi_6^2+\psi_2^2\psi_6^2$$
$$\psi_1^2\psi_4^2+\psi_3^2\psi_6^2+\psi_2^2\psi_5^2$$
$$\psi_1^2\psi_6^2+\psi_2^2\psi_3^2+\psi_4^2\psi_5^2$$

It follows that G, to fourth-order, is of form

$$G = G_o + A\eta^2 + [C_1 + (\gamma_1^2\gamma_2^2+\gamma_3^2\gamma_4^2+\gamma_5^2\gamma_6^2)C_2 + (\gamma_1^2\gamma_3^2+\gamma_3^2\gamma_5^2+\gamma_1^2\gamma_5^2 +\gamma_2^2\gamma_4^2+\gamma_4^2\gamma_6^2+\gamma_2^2\gamma_6^2)C_3 + (\gamma_1^2\gamma_4^2+\gamma_3^2\gamma_6^2+\gamma_2^2\gamma_5^2)C_4 + (\gamma_1^2\gamma_6^2+\gamma_2^2\gamma_3^2+\gamma_4^2\gamma_5^2)C_5]\eta^4.$$

This form for the Gibbs free energy was also found to be appropriate to X-point of Fm3m (as discussed before) and Im3m.[42] As was previously found to be the case for X-point, between discrete solutions, there are three continuous solutions with variable contributions from several basis functions.

The solutions can be characterized in terms of the basis functions as follows:

$1/\sqrt{2}(\psi_1+\psi_2)$: Fmmm discrete solution

$\gamma_1\psi_1+\gamma_2\psi_2+\gamma_4\psi_4$: $P2_1/c$ continuous solution

$1/\sqrt{2}(\psi_1+\psi_4)$: P4/mbm discrete solution

$\gamma_1\psi_1+\gamma_4\psi_4+\gamma_6\psi_6$: Pnma continuous solution

$1/\sqrt{2}(\psi_1+\psi_6)$: P4/nmm discrete solution

$\gamma_1\psi_1+\gamma_2\psi_2+\gamma_6\psi_6$: $P2_1/m$ continuous solution

These unusual solutions permit consecutive second-order transition from Fm3m to P4/nmm symmetry at some temperature, and continuation to Pnma or $P2_1/m$ (corresponding to non-zero values for γ_1, γ_4 and γ_6 or γ_1, γ_2 and γ_6 respectively) at some lower temperature.

This kind of possible thermal symmetry breaking has not been observed in NaCl-type transitions, however, as has been demonstrated here, it is consistent with Landau theory in cubic cases with two-dimensional small representations and three independent k wave vectors.

All the possible structures from second-order transition from NaCl-type are summarized with examples in Table 7.

Table 7. Allowed structures arising continuously from the NaCl-type

Symmetry point	k vectors	Space group	Space Lattice parameters	Atom positions	Examples
Γ	0	R3m	$a \simeq a^o/\sqrt{2}$	0, 0, 0 (1)	NiO(43)
			$\alpha \simeq 60°$	$1/2+\delta, 1/2+\delta, 1/2+\delta$ (1)	FeO(44)
					MnO(45)
		I4mm	$a \simeq a^o/\sqrt{2}$	0, 0, 0 (2)	CoO(45)
			$c \simeq a^o$	0, 0, $1/2+\delta$ (2)	
X	a^*, b^*, c^*	P4/nmm	$a \simeq a^o/\sqrt{2}$	$1/4, 1/4, 1/4+\delta$ (2)	
			$c \simeq a^o$	$1/4, 1/4, 3/4+\varepsilon$ (2)	
		Cmcm	$a \simeq a^o$	$0, 1/4+\delta, 1/4$ (4)	
			$b \simeq a^o$	$0, 3/4+\varepsilon, 1/4$ (4)	
			$c \simeq a^o$		
		Pnmm	$a \simeq a^o/\sqrt{2}$	$1/4, 1/4, 1/4+\delta$ (2)	CrN(46)
			$b \simeq a^o$	$1/4, 3/4, 1/4+\varepsilon$ (2)	
			$c \simeq a^o/\sqrt{2}$		
		$P2_13$	$a \simeq a^o$	δ, δ, δ (4)	FeSi(47)
				$1/2+\varepsilon, 1/2+\varepsilon, 1/2+\varepsilon$ (4)	
		$P\bar{4}3m$	$a \simeq a^o$	$1/4+\delta, 1/4+\delta, 1/4+\delta$ (4)	
				$3/4+\delta, 3/4+\delta, 3/4+\delta$ (4)	
		R32	$a \simeq a^o$	0, 0, 0 (1)	
			$\alpha \simeq 90°$	$0, 1/2+\delta, -1/2-\delta$ (3)	
				1/2, 1/2, 1/2 (1)	
				$1/2, \varepsilon, -\varepsilon$ (3)	

Table 7 (continued)

Symmetry point	k vectors	Space group	Space Lattice parameters	Atom positions	Examples
X		$P4_2/mnm$	$a \simeq a^o$	$1/4+\delta, 1/4+\delta, 0$ (4)	
			$b \simeq b^o$	$1/4-\varepsilon, 3/4-\varepsilon, 0$ (4)	
			$c \simeq c^o$		
		P4/nmm	$a \simeq a^o$	0, 0, 0 (2)	
			$b \simeq b^o$	$0, 1/2, 1/2+\delta$ (2)	
			$c \simeq c^o$	0, 0, 1/2 (2)	
				$0, 1/2, \varepsilon$ (2)	
		$P2_1/m$	$a \simeq a^o$	$0+\delta, 1/4+\varepsilon, 1/4$ (2)	
			$b \simeq b^o$	$1/2+\delta, 3/4+\varepsilon, 1/4$ (2)	
			$c \simeq c^o$	$0+\delta, 3/4+\varepsilon, 1/4$ (2)	
			$\gamma \simeq 90°$	$1/2+\delta, 1/4+\varepsilon, 1/4$ (2)	
		$P2_1/b$	$a \simeq a^o$	0, 0, 0 (2)	
			$b \simeq b^o$	1/2, 0, 0 (2)	
			$c \simeq c^o$	0, 1/2, 0 (2)	
			$\gamma \simeq 90°$	1/2, 1/2, 0 (2)	
		$Pmn2_1$	$a \simeq a^o$	$0, 0+\delta, 0+\varepsilon$ (2)	
			$b \simeq b^o$	$0, 1/2+\delta, 1/2+\varepsilon$ (2)	
			$c \simeq c^o$	$0, 0+\delta, 1/2+\varepsilon$ (2)	
				$0, 1/2+\delta, 0+\varepsilon$ (2)	

Table 7 (continued)

Symmetry point	k vectors	Space group	Space Lattice parameters	Atom positions	Examples
L	$(a^*+b^*+c^*)/2$ $(a^*+b^*-c^*)/2$ $(a^*-b^*+c^*)/2$ $(-a^*+b^*+c^*)/2$	$R\bar{3}m$	$a \simeq \sqrt{3}/2a^o$ $\alpha \simeq \cos^{-1}5/6$	0, 0, 0 (1) 1/2,1/2,1/2 (1)	$Sc_{1-x}S$(3) $Zr_{1-x}S$(40)
		Fm3m	$a \simeq 2a^o$	0, 0, 0 (4) 1/2,1/2,1/2 (4) 0, 1/4,1/4 (24) 1/4,1/4,1/4 (8) 1/4+δ, 0, 0 (24)	
		Fd3m	$a \simeq 2a^o$	0, 0, 0 (16) 1/2,1/2,1/2 (16) 1/4+δ,1/4+δ,1/4+δ(32)	$Y_{1-x}Se$(48) Zr_3S_4(49)
		C2/m	$a \simeq \sqrt{3}/2a^o$ $b \simeq a^o/\sqrt{2}$ $c \simeq \sqrt{3}/2a^o$ $\beta \simeq \cos^{-1}-1/3$	0, 0, 0 (2) 0, 1/2,1/2 (2) 1/4+δ, 0, 3/4+ε(4)	AuSe(50)
		C2/c	$a \simeq \sqrt{3}/2a^o$ $b \simeq a^o/\sqrt{2}$ $c \simeq \sqrt{3}/2a^o$ $\beta \simeq \cos^{-1}-1/3$	1/4,1/4, 0 (4) 0,1/4+δ,1/4 (4)	
		C2/m	$a \simeq 2a^o$ $a \simeq 2b^o$ $c \simeq 2c^o$ $\beta \simeq 90°$	(a)[a], (b), (c), (d), (e) (f), 2(i), (j); (j), (h) (g), 4(i)	

[a]Wyckoff notation.

Table 7 (continued)

Symmetry point	k vectors	Space group	Space Lattice parameters	Atom positions	Examples
		C2/c	$a \simeq 2a^o$ $a \simeq 2b^o$ $c \simeq 2c^o$ $\beta \simeq 90°$	(a), (b), (c), 3(d), (f); 2(e), 3(f)	
W	$\pm(\mathbf{a}^*+\mathbf{b}^*/2)$ $\pm(\mathbf{b}^*+\mathbf{c}^*/2)$ $\pm(\mathbf{c}^*+\mathbf{a}^*/2)$	I4/mmm	$a \simeq a^o$ $c \simeq 2a^o$	0, 0, 0 (2) 0, 0, 1/2 (2) 0, 1/2, 1/4 (4) 0, 0, 1/4+δ (4) 0, 1/2, 0 (4)	NbN_{1-x}(51)
		Pm3n	$a \simeq 2a^o$	0,1/4+δ,1/4+ε (24) 1/4+α, 0, 0 (12) 1/4,1/4,1/4(8) 1/4, 0, 1/2 (6) 0, 1/4,1/2 (6)	
		Pmma	$a \simeq a^o$ $b \simeq a^o$ $c \simeq 2a^o$	(a), (d), (e), (f); (b), (c), (e), (f)	
		Fmmm	$a \simeq \sqrt{2}a^o$ $b \simeq \sqrt{2}a^o$ $c \simeq 2c^o$	0, 0, 0 (4) 0, 0, 1/2 (4) 1/4,1/4,1/4 (8) 1/4, 1/4, 0 (8) 1/4+δ, 0, 0 (8)	

Table 7 (continued)

Symmetry k vectors point	Space group	Space Lattice parameters	Atom positions	Examples
	P4/mbm	$a \simeq 2a^o$ $c \simeq c^o$	(a), (d), (j), (g); (a), (c), (d), (i); (b), (c), (e), (i)	
	P4/nmm	$a \simeq 2a^o$ $c \simeq c^o$		
	Pa3	$a \simeq 2a^o$	(a), (b), (d); (c), (d)	
	$P2_1/c$	$a \simeq a^o$ $b \simeq 2b^o$ $c \simeq 2c^o$ $\beta \simeq 90°$	(a), (b), 3(e); (b), (d), 3(e)	
	$P2_1/m$	$a \simeq 2a^o$ $b \simeq 2b^o$ $c \simeq c^o$ $\beta \simeq 90°$	(a), (b), 4(e), (f); (c), (d), 4(e), (f)	
	Pnma	$a \simeq 2a^o$ $b \simeq 2b^o$ $c \simeq 2c^o$	(b), (a), 4(c), (d); 4(c), 2(d)	
	$R\bar{3}m$	$a \simeq 2a^o$ $\alpha \simeq 90°$	(a), (b), (d), (e), 2(h), (g), (f); (c), 3(h), (i)	

EXPERIMENTAL

Synthesis

Transition metal sulfides and selenides

The binary compounds, Zr-S, Y-Se and Lu-S, were prepared by heating mixtures of metal strips and elemental sulfur or selenium. The metals were obtained from Ames Laboratory (99.9% purity), and sulfur powder and selenium shot were obtained from Alfa Ventron (99.999% purity). The desired amounts of metals and nonmetals (for the samples with starting composition in the range X/M=0.9~1.5, where X=S or Se and M=Zr or Y or Lu) were placed in fused silica tubes which were previously outgassed using an oxygen-gas torch. The sample tubes were evacuated to about 10^{-6} Torr. residual pressure, sealed and heated for several days in a tube furnace. The temperature was raised gradually from 450° to 850°C. When the sulfur (selenium) was no longer visible in the tubes, the products were sulfur (selenium) rich compounds coating the outside of unreacted metal strips. To achieve equilibrium more rapidly, the samples were ground, pelletized, and annealed under high vacuum (10^{-6} Torr) at about 1400~1750°C in an inductively heated tungsten Knudsen cell. The temperatures were estimated using optical pyrometer measurements.

Transition metal nitride

The NbN_{1-x} samples were synthesized by heating a Nb foil in a slowly flowing equivolume mixture of NH_3 and N_2 at temperatures in the neighborhood of 1300°C. The niobium foil was obtained from Alfa Ventron

(99.8% purity) and the ammonia and nitrogen gases were 99.999% pure (with less than 2 ppm of oxygen content). The foil was held in a tube that was initially Ta and finally Ta_2N. This tube was heated inductively using an induction coil external to a water cooled fused silica enclosure.

Powder Diffraction

Guinier x-ray powder diffraction

For the initial phase analysis of the sample, the x-ray powder patterns were taken using a Guinier Camera (Enraf Nonius or IRDAB XDC-700) provided with Cu K_α (λ=1.54056Å) radiation, silicon powder (NBS Standard Reference Material 640a) was mixed with the sample and used as a standard.

High-temperature x-ray diffraction

The structures and phase transitions were studied using a Rigaku θ-θ powder diffractometer equipped with a Bühler sample chamber and controlled high-temperature power supply. The sample chamber consists of a cylindrical, doubled-walled, water cooled pot made of stainless steel with an irradiation window of beryllium and a lid carrying two pairs of electrodes for heating the samples directly and by radiation. The residual pressure inside the chamber was held in the low 10^{-6} Torr. region using a turbomolecular pump which was attached as close as possible to the chamber to maximize pumping efficiency. The sample chamber was connected to a glove box which was filled with nitrogen gas to protect the sample and chamber from moisture. Usually the samples

were held on a Mo holder and the temperatures were measured using WRe-thermocouples. The temperature can be controlled from room temperature up to 2000°C.

Data collection

Cu K_α radiation was used and the diffracted beam was monochromatized using a graphite exit monochromator. The diffractometer data were taken using θ-θ stepscan procedure and the step size was 0.02° in 2θ. The counting time used was 960 second per degree(θ).

X-ray diffraction data analysis

For structure analysis, a full-profile pattern fitting Rietveld-type program KDBW,[52] a local modification of the original DBW 3.2,[53] was used. The local modification from Dr. Jacobson's group includes: i) adoption of several additional profile functions, ii) sample area correction, iii) improved preferred orientation correction and iv) better least-squares, the maximum neighborhood method.

The refined structure was obtained from the powder data assuming mixed $K_{\alpha1}$-$K_{\alpha2}$ radiation. Generally parameters refined for each diffraction data analysis were: scale factor, unit cell parameters, background parameters, atomic positions, zero point, overall isotropic thermal parameters or individual isotropic thermal parameters, the profile shape parameters, peak half-width parameters, occupation parameters and the sample area correction parameters. The Pearson VII function was used to describe peak shapes in this research, since these peak shapes were typically between Gaussian and Lorentzian.

The definitions of various R factors which were cited in this research are as follows:

$R_b = \Sigma|\sqrt{I_B}\ (obs) - \sqrt{I_B}(calc)| \ / \ \Sigma\sqrt{I_B}(obs)$; the Bragg R factor

$R_p = [\Sigma(Y_i\ (obs) - 1/c\ Y_i\ (calc))] \ / \ \Sigma Y_i\ (obs)$; the pattern R factor

$R_{wp} = [\ \Sigma w_i\ (Y_i\ (obs) - 1/cY_i\ (calc))^2 \ / \ \Sigma\omega_i\ (Y_i\ (obs))^2]^{1/2}$; the weighted pattern R-factor

where I_B is the intensity assigned to a particular Bragg reflection, Y_i is the intensity observed at the ith step in the step-scanned pattern, c is a scale factor and w_i is the weight. R_b closely resembles the "conventional" R factor widely used in single-crystal structure analysis. R_{wp} is the quantity that is actually minimized in the least squares refinement procedure.

In much, but not all, of this research, single-crystal studies were not possible because of the nature of the formation of process in which multiple twinning predominated. However, because the starting models can be severely restricted using the Landau-theory of symmetry and phase transitions, it was possible to solve a number of distorted and ordered structures by combining high-temperature x-ray diffraction and Rietveld-type full-profile refinement.

Single-crystal technique

The single-crystal data were collected with an Enraf-Nonius CAD4 four-circle diffractometer (for Y_5S_7) or with a Rigaku AFC6 rotating

anode four-circle diffractometer (for Cr_2N) and monochromated Mo K_α radiation. Additional details are described in section on the individual compounds.

Composition Analysis

Final compositions of the sulfides and selenides under consideration were investigated by oxidizing to their highest oxidized form in a Pt crucible in air at about 900°C. The composition of NbN_{1-x} was determined by vacuum fusion analysis in addition to combustion analysis.

SECTION I. ORDER-DISORDER TRANSITION, AND STRUCTURES OF THE NONSTOICHIOMETRIC MONOSULFIDES OF ZIRCONIUM

INTRODUCTION

The nonstoichiometric monosulfides of zirconium have been studied by a number of groups since the earliest investigation of defect NaCl-type structure of $Zr_{1-x}S$ by Strotzer et al. (1939).[5] Hahn et al. (1951)[49] prepared a phase labeled Zr_3S_4 and proposed it to be cubic a=10.25Å, in which half of the metal sites were fully occupied and half were statistically occupied. It was suggested by Jellinek (1963)[6] that the superstructure of ZrS might have an ordered cubic superstructure based on the NaCl-type structure or a slight rhombohedral distortion of the cubic lattice. McTaggert and Wadsley[54] found that a defect NaCl-structure of $ZrS_{0.9}$~$ZrS_{1.6}$ has a primitive cell of 10.25Å. Nguyen[55] examined the phases at a variety of compositions and reported that Zr_2S and WC type coexist when S/Zr=0.88, WC type alone occurs for S/Zr=0.9 and 0.99, WC type coexists with the NaCl-type superstructure when S/Zr=1.05 and 1.21, and the NaCl-type superstructure occurs alone for S/Zr=1.28 and 1.30. Conard and Franzen investigated a single crystal of $Zr_{0.77}S$ to determine the nature of the ordering, and a monoclinic superstructure was found.[8] Furthermore, defect ZrS has been found to be a superconductor,[16] and electron diffraction results[56] showed a 2x2 superstructure together with ordering in every third plane perpendicular to the $\bar{1}$ 1 0 rhombohedral direction. This result is very similar to that found for $Sc_{1-x}S$.[3]

RESULTS

In this research, a sample with the composition S/Zr=1.34 was prepared and the structure was investigated using the high-temperature x-ray diffractometer at temperatures up to 1500°C. At temperatures below 1250±20°C the NaCl-type superstructure was observed, while for higher temperatures the x-ray diffraction was that of NaCl-type alone, except that after a few hours at the highest temperatures the WC-type pattern was observed to grow into diffractometer data.

A sample with S/Zr=1.34 was examined at room temperature and the data were analyzed by Rietveld analysis. A fit to a superstructure of the $CdCl_2$ type with $R\bar{3}m$ symmetry was obtained (profile R=12.9%, derived Bragg R factor=4.6%). Two weak impurity lines at 2θ=28.7 and 31.6° were identified as the two strongest diffraction lines of monoclinic ZrO_2, indicating that the zirconium sulfide sample was slightly surface oxidized at high temperature even though the residual pressure at the sample was less than 10^{-6} Torr. The following parameters were refined: overall scale factors, zero-point, hexagonal a and c in $R\bar{3}m$, peak half-width, the profile parameters, background, sample area, sulfur position parameters. The zirconium positions are fixed, and the refined sulfur positions did not vary from their locations in the cubic structure. The final refined structural parameters in the hexagonal cell are given in Table 8.

The rhombohedral lattice parameters are α=33.377(3)° and a=6.3194(6)Å (see Figure 2). The occupation parameters are in excellent agreement with the combustion analysis results which yielded

S/Zr=1.34(1). The model fits the data well not only in the sense of a low Bragg R value (see Table 9 for I_{obs} and I_{calc}), but also in the sense of fitting the split and weak peaks relative to the cubic structure. The calculated and observed diffraction patterns are shown in Figure 3.

Table 8. Refined parameters for $Zr_{1-x}S$ in the hexagonal[a]

Atom	Position	Fractional Occupancy	Thermal
Zr(a)[b]	x=0, y=0, z=0	1.05(5)	0.7(3)
Zr(b)	x=0, y=0, z=1/2	0.50(2)	0.8(3)
S(c)	x=0, y=0, z=0.249(1)	1.0	0.3(3)

[a]Unit cell : a=3.6295, c=17.885(2) Å.
[b]Wyckoff notation.

The room temperature Guinier powder diffraction pattern of a sample with S/Zr=1.37 was found to exhibit three very weak (barely discernible) diffraction lines at 2θ=16.73, 18.32, 22.61°. These lines could be indexed using the cell that results from tripling the periodicity along the $\bar{1}10$ direction, yielding a monoclinic (pseudoorthorhombic) cell with a=10.86Å, b=6.28Å, and c=17.88Å and α, β, and γ all essentially 90°.

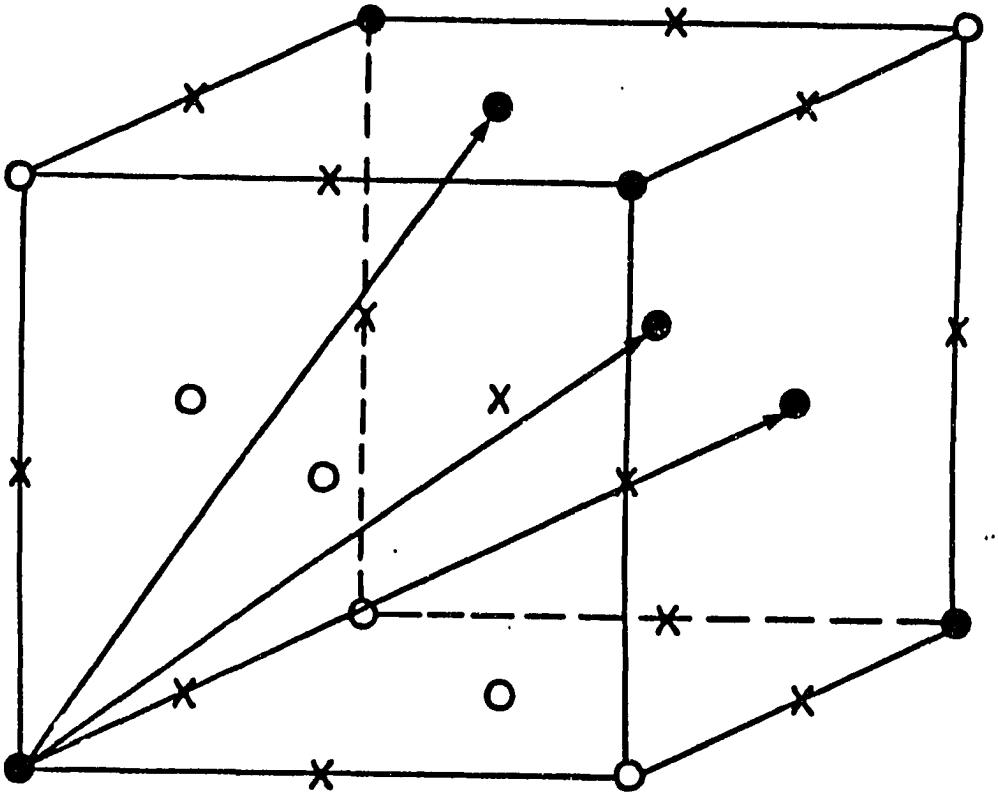

FIGURE 2. The cubic unit cell of substructure NaCl-type zirconium monosulfide and the inscribed rhombohedral cell that results from ordering of metal vacancies in alternate planes along the 111 direction (differentiated by open and dark circles). The rhomboheral angle would be 33.56° if there were no relaxation of the cubic lattice

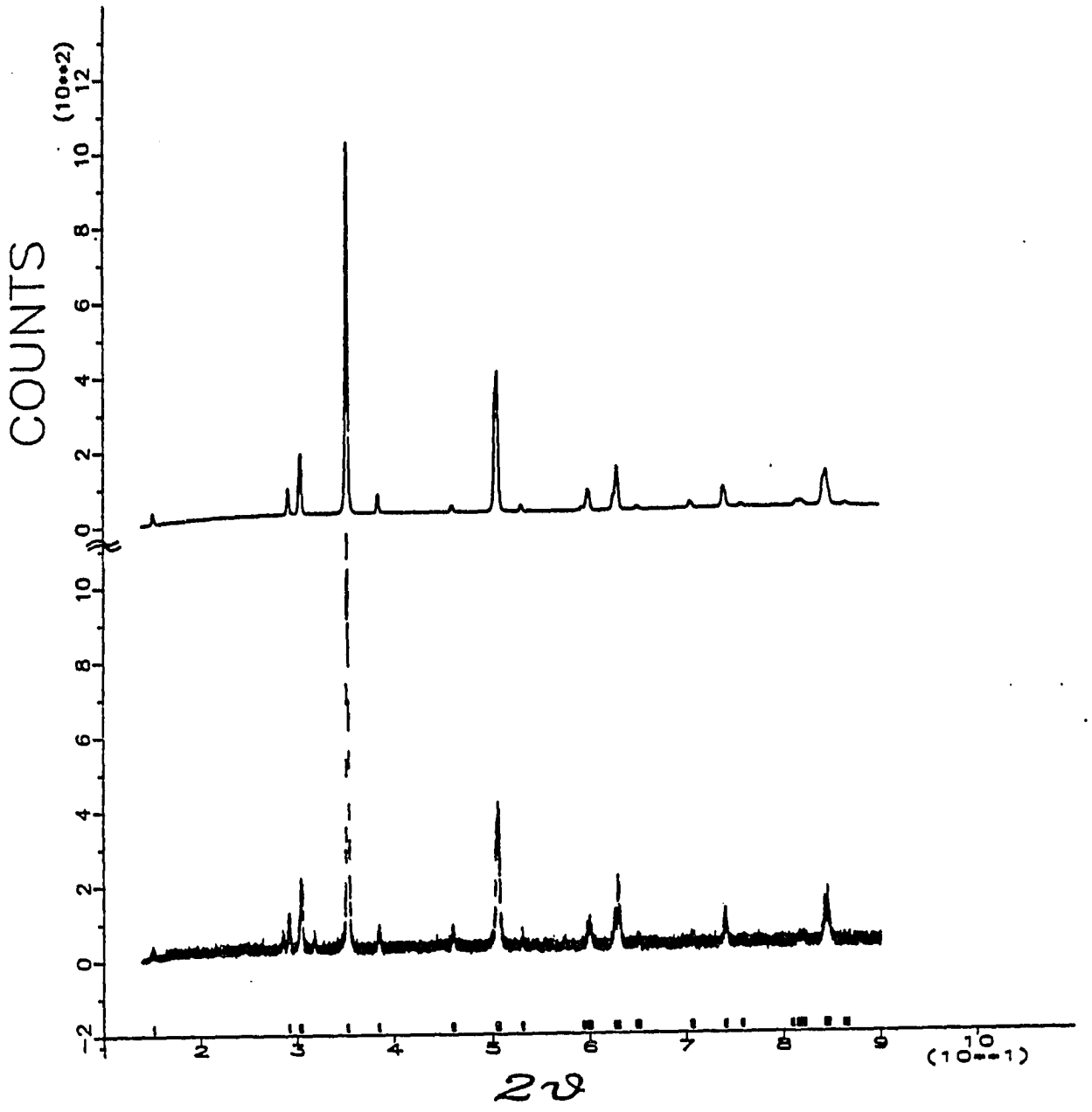

Figure 3. Calculated (top) and observed (bottom) powder diffraction profile of $Zr_{0.75}S$. Vertical strokes indicate calculated Bragg-peak position

Table 9. Calculated 2θ values and calculated and observed intensities for $Zr_{1-x}S$ lines identified by hexagonal indexing

h k l (hex)	2θ (α_1 and α_2)	I_{calc} (x10^{-5})	I_{obs} (x10^{-5})	superstructure reflections
1 0 1	28.82	8.48	9.31	x
1 0 1	28.99	4.23	4.61	x
0 0 6	29.95	5.16	5.27	
0 0 6	30.03	2.57	2.65	
0 1 2	30.11	1.54	1.58	
0 1 2	30.19	0.76	0.79	
1 0 4	34.86	102.	108.	
1 0 4	34.95	50.6	53.8	
0 1 5	38.08	4.88	4.94	x
0 1 5	38.18	2.43	2.45	x
0 0 9	45.61	0.99	1.11	x
1 0 7	45.72	2.44	2.72	x
0 0 9	45.73	0.49	0.55	x
1 0 7	45.84	1.21	1.35	x
0 1 8	50.02	33.5	32.8	
0 1 8	50.15	16.7	16.4	
1 1 0	50.23	33.1	32.4	
1 1 0	50.36	16.4	16.1	
1 1 3	52.68	3.28	3.15	x
1 1 3	52.82	1.63	1.57	x
0 2 1	58.95	1.19	1.16	x
0 2 1	59.14	0.59	0.58	x
1 0 10	59.41	2.48	2.45	
1 0 10	59.57	1.23	1.22	
1 1 6	59.60	4.90	4.87	
2 0 2	59.69	2.43	2.44	
1 1 6	59.75	2.43	2.45	

Table 9 (continued)

h k l (hex)	2θ (α_1 and α_2)	I_{calc} (x10^{-5})	I_{obs} (x10^{-5})	superstructure reflections
2 0 2	59.85	1.21	1.21	
0 0 12	62.24	5.47	6.05	
0 0 12	62.40	2.72	3.00	
0 2 4	62.60	16.11	17.88	
0 2 4	62.77	8.01	8.93	
0 1 11	64.47	0.77	0.81	x
0 1 11	64.64	0.38	0.40	x
2 0 5	64.74	0.92	0.96	x
2 0 5	64.91	0.46	0.48	x
1 1 9	70.17	1.49	1.56	x
0 2 7	70.26	0.61	0.64	x
1 1 9	70.37	0.74	0.78	x
0 2 7	70.45	0.30	0.32	x
2 0 8	73.61	9.66	10.02	
2 0 8	73.82	4.80	4.98	
1 0 13	75.35	0.63	0.65	x
1 0 13	75.56	0.31	0.33	x
0 0 15	80.48	0.12	0.13	x
0 0 15	80.72	0.06	0.06	x
2 1 1	81.06	0.89	0.91	x
0 1 14	81.21	0.85	0.88	
2 1 1	81.29	0.44	0.45	x
0 1 14	81.45	0.43	0.44	
0 2 10	81.46	0.84	0.87	
0 2 10	81.69	0.42	0.43	
1 2 2	81.70	1.67	1.72	
1 2 2	81.94	0.83	0.86	

Table 9 (continued)

h k l (hex)	2θ (α_1 and α_2)	I_{calc} (x10^{-5})	I_{obs} (x10^{-5})	superstructure reflections
1 1 12	83.95	13.4	13.9	
1 1 12	84.19	6.70	6.89	
2 1 4	84.27	13.33	13.73	
2 1 4	84.52	6.64	6.82	
2 0 11	85.95	0.33	0.33	x
1 2 5	86.19	0.80	0.81	x
2 0 11	86.20	0.16	0.17	x
1 2 5	86.45	0.40	0.40	x

DISCUSSION

The metal deficient monosulfide exists for a narrow range of stoichiometry about the composition given by S/Zr=1.32. The vacancies order at lower temperature, and this ordering corresponds to the L point of Brillouin zone. Among the possible solutions from Landau theory the solution corresponding to $R\bar{3}m$ ordering is easily chosen based on the splitting of lines and extra lines (relative to NaCl-type) in a Guinier powder pattern. This compound occurs in a structure that can be described rather accurately as $CdCl_2$ type ($R\bar{3}m$ symmetry), a superstructure that arises from a vacancy ordering in alternate planes perpendicular to the body diagonal of a cubic NaCl-type cell. There is a slight relaxation (from $\alpha=33.56^{o}$ in the cubic structure to $\alpha=33.38^{o}$ in the rhombohedral structure). The vacancies in this structure order weakly within the planes, and this ordering triples the periodicity along the $\bar{1}10$ rhombohedral direction. These results are in good agreement with those from electron diffraction experiments[56] and show a remarkable similarity to those found for $Sc_{1-x}S$.

A question that remains is the identity of the previously reported monoclinic $Zr_{0.77}S$ structure. It appears likely that this structure is closely related to that which results from the secondary ordering along the $\bar{1}10$ direction of the rhombohedral lattice. Since the superstructure reflections reported in reference (8) were very weak, the reported monoclinic structure could be in error, a suggestion that was made previously.[3] Furthermore, the reported structure was based on data from a single crystal, and it is possible when studying ordering processes to

obtain individual single-crystals in which the ordering is not that characteristic of the bulk. Accordingly, it is concluded here that the best description of the ordering in bulk $Zr_{1-x}S$ is that it occurs initially in alternate planes along the cubic body diagonal at about 1250°C. Since this ordering can, by symmetry arguments presented in the previous chapter, occur via a second-order transition, and since the results gave no evidence of a two-phase mixture, it is suggested that this ordering transition is second-order. There is then a further weak ordering along the $\bar{1}10$ direction so as to triple the periodicity in this direction.

SECTION II. INVESTIGATION OF THERMAL SYMMETRY-BREAKING TRANSITION IN NbN_{1-x}

INTRODUCTION

The Nb-N system in the vicinity of the mononitride has been studied previously by Brauer and Esselborn[10] and Guard, Savage and Swarthout.[11] The thermal behavior of nitrogen deficient niobium mononitride has been investigated by neutron diffraction[12] and c/a variation with temperature indicates a continuous structure change from cubic to tetragonal when the temperature is lowered 1400°~1600°C (with the temperature of the transition depending upon the N/Nb ratio). The structure reported by Christensen from neutron diffraction[12] does not fit this observation. A more recent neutron diffraction result yielded a tetragonal cell with $a=b=a^{o}$, $c=2a^{o}$ and I4/mmm symmetry, in agreement with the conclusion reached below.

RESULT AND DISCUSSION

The NbN_{1-x} samples were synthesized by the method discussed previously. The product was analyzed by photoelectron spectrum, vacuum fusion and combustion analysis. No extraneous metal peaks (e.g. peaks from Ta arising from interaction with the sample holder) were observed in the photoelectron spectrum. The vacuum fusion analysis yielded 1600 ppm oxygen and 3100 ppm hydrogen. Mass gain upon synthesis and upon combustion in air to Nb_2O_5, when corrected for the O and H impurity, both yielded N/Nb=0.77. The hydrogen was removed by outgassing the sample in high vacuum at 1500°C.

The final procedures (several samples were studied, but the technique was refined and applied to the final sample) were as follows:

1) a sample was prepared at 1300°C in an equimolar mixture of N_2 and NH_3 at a pressure of 1 atm for several hours,
2) the sample was analyzed by room temperature Guinier x-ray diffraction and only tetragonal NbN_{1-x} was found to be present at the x-ray level of detection,
3) the sample was finely ground and placed in the diffractometer chamber,
4) the temperature was raised to 1500°C until outgassing was completed,
5) the sample was systematically cooled to room temperature, periodically scanning over the peaks that originated in the cubic 3, 1, 1 peak,

6) diffraction data were collected from the sample cooled to room temperature for $20^{o} \leq 2\theta \leq 95^{o}$ during a 9 hour scan,

7) the room temperature diffraction data were used in a Rietveld full-profile refinement, as discussed in this section.

The previous report[12] of the cubic to tetragonal transition in NbN_{1-x} indicates a continuous variation of c/a toward unity with increasing temperature, and stability of the cubic form at high temperature. In this work a continuous coalescence of the peaks originating in the cubic 3, 1, 1 family was observed in agreement with this result. Thus the high-temperature x-ray diffraction patterns of NbN_{1-x} confirmed the apparent symmetry-breaking character of the transition, i.e., the approach of c/a toward unity as the temperature approached 1200°C. Accordingly, the structures corresponding to the various irreducible representations of Fm3m symmetry were examined. It was clear from the outset that the low temperature diffraction pattern could be indexed on a tetragonal basis, and thus irreducible representations leading to the tetragonal symmetry were examined. It was also clear, because of the existence of superstructure reflections, that the irreducible representation in question is at some reciprocal space point other than k=0, thus the solutions at X, L, or W yielding tetragonal symmetry were considered.

As shown in the earlier discussion three tetragonal space-groups are found at W point: I4/mmm, P4/mbm and P4/nmm ($a=2a^{o}$, $c=a^{o}$). Also there are three tetragonal space-groups at the X point: P4/nmm ($a=a^{o}/\sqrt{2}$, $c=a^{o}$), $P4_2/mmm$ and P4/nmm($a\simeq b\simeq a^{o}$, $c=a^{o}$).

There are five weak superstructure reflections (at 2θ=20.5°, 28.8°, 37.3°, 57.0° and 80.6°) observed in the diffraction pattern of tetragonal NbN_{1-x} (see Figure 4). All the possible tetragonal solutions were considered, and only the structure with I4/mmm symmetry yields calculated Bragg diffraction for all five superstructure reflections. An essential feature in obtaining a satisfactory fit to the superstructure data is the variation of the z parameter of the Nb position in I4/mmm away from the NaCl-type value of 1/4. If the Nb positions are fixed at the NaCl-type positions, no observable intensity is calculated for the three higher angle superstructure reflections. The final refined parameters for the NbN_{1-x} structure are given in Table 10 and the structure is shown in Figure 5.

Table 10. Refined Parameters for NbN_{1-x} in Tetragonal Cell[a]

Atom	Site symmetry	x	y	z	Fractional Occupancy
N1	4/mmm	0	0	0	0.08
N2	4/mmm	0	0	1/2	1.00
N3	$\bar{4}$m2	0	1/2	1/4	1.00
Nb1	4mm	0	0	0.24373	1.00
Nb2	mmm	0	1/2	0	1.00

[a] a=4.3860(2), c=8.6606(5), R=13.93%, R_w=18.90%, Bragg R=2.97%.

The refined structure in I4/mmm differs from that in I$\bar{4}$m2 only in the fixed position of the Nb atom at 0 1/2 0 (which was at 0 1/2 0.0034

in the structure refined in $I\bar{4}m2$).[10] The refinement I4/mmm yielded R values equivalent to those obtained in $I\bar{4}m2$, and thus this is the preferred description.

The space group $I\bar{4}m2$ could result from a distortion corresponding to an irreducible representation of I4/mmm at k=0 compatible with the totally symmetric irreducible representation of Fm3m at W point, and thus a continuous symmetry breaking to $I\bar{4}m2$ through I4/mmm would be possible. Such distortion is not required by the observed data.

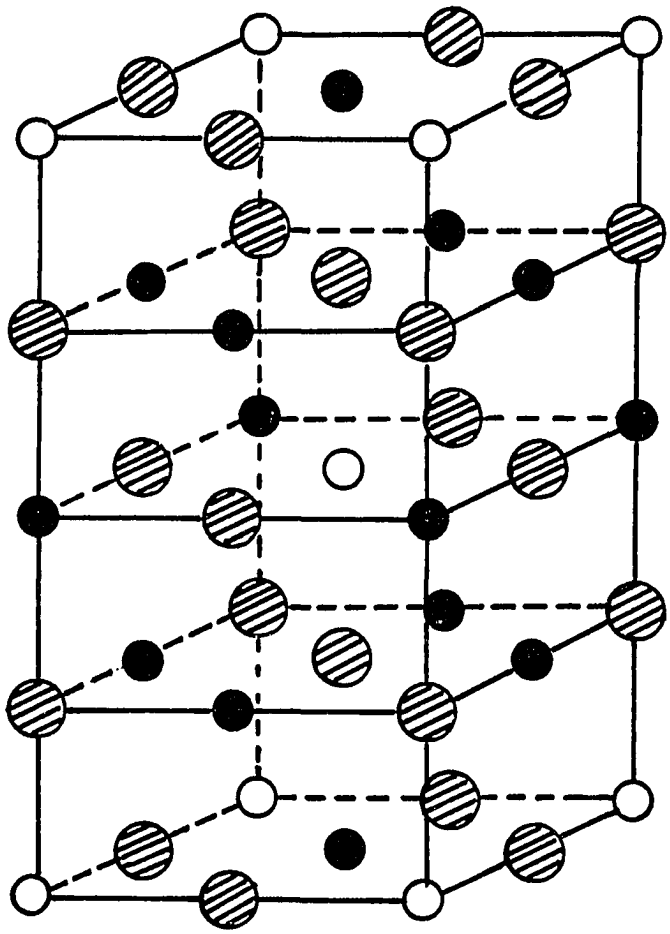

Figure 4. The structure of NbN_{1-x}. Hatched circles indicate nibium atom positions and filled circles indicate nitrogen atom positions. Open circles are partly filled nitrogen atom positions

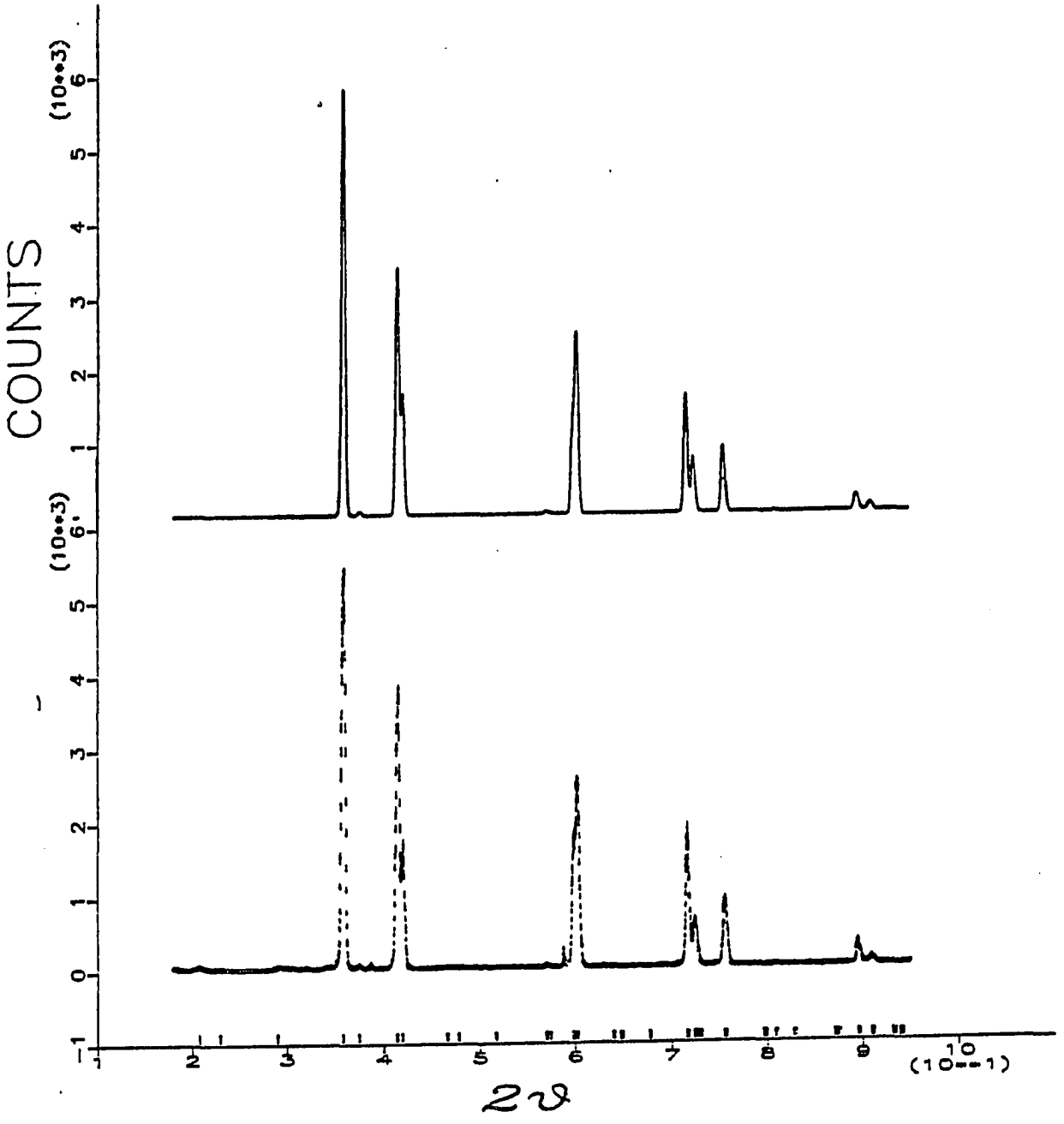

Figure 5. Comparison of calculated (top) and observed (bottom) powder diffraction for NbN_{1-x}. Vertical strokes indicate calculated Bragg-peak positions. The diffractions at 39° and 59° are from Nb_2N and the sample holder, respectively

CONCLUSION

The powder x-ray diffraction data for NbN_{1-x} (x=0.23) have been interpreted with the aid of Landau theory and Rietveld full-profile refinement to yield the structure of low-temperature tetragonal from of nitrogen deficient niobium mononitride. The space group is I4/mmm and the lattice parameters are: a_{tet}=4.386(Å)≃a^o and c_{tet}=8.661Å≃$2a^o$. The vacancies are ordered in alternate N-containing planes and ABAB··· stacking of the planes. There is also a slight relaxation of Nb positions relative to NaCl-type positions along the c direction.

SECTION III. VACANCY ORDERING IN $Y_{1-x}Se$

INTRODUCTION

The compound YSe has been observed to have the NaCl-type structure with a wide range of homogeneity, and Y_2Se_3 has been observed to be isostructural with Sc_2S_3 with space group Fddd as reported by Dismukes and White.[57]

During the investigation of a nonstoichiometric phase between YSe and Y_2Se_3, a defect, vacancy ordered phase relating to NaCl-type structure was found.

RESULT AND DISCUSSION

A sample with initial composition Se/Y=1.3 was prepared as previously described. The sample quenched from 1450°C (using induction heating) provided a simple powder pattern of the NaCl-type structure. This sample, when annealed at about 600°C for two weeks and cooled slowly to room temperature over several days, gave evidence of vacancy ordering. The structure and order-disorder transition of $Y_{1-x}Se$ were studied using high-temperature x-ray diffraction at temperatures up to 400°C. At temperatures below 275°±25°C the ordered structure was observed, while for the higher temperatures the simple NaCl-type x-ray diffraction pattern was observed.

The $R\bar{3}m$ vacancy ordering found for $Zr_{1-x}S$ and $Sc_{1-x}S$ does not provide a fit to the diffraction pattern observed for $Y_{1-x}Se$ (figure 6). However, the positions of all observed superstructure diffractions were fit by both the Fm3m and Fd3m symmetries with a cell twice that of parent cubic cell. In an attempt to distinguish between these two models the structure was refined in both the Fm3m and Fd3m space groups and the results were compared (Table 11). The Rietveld full-profile refinement procedure was used.

The observed superstructure reflections were of such low intensity that the usual R factors for the two structural models were the same for the two models. The profile R=13.7% and the derived Bragg R=4.2%.

However, the thermal parameters are substantially different for the two models (Table 11) providing an indication that the Fd3m model is closer to the correct structure. This conclusion is also favored by the

lack of some superstructure reflections, for example, at 2θ=35.2, which is the location of the 0 2 4 reflection which is allowed for Fm3m but not for Fd3m. The refined lattice parameter is 11.4211(4)Å.

This nonstoichiometric material has a structure which is closely related to $Ca_{33}Ge$ structure (The structure of Ti_2C) as described in Figure 7.

The superstructure reflections were not observed in a sample at temperatures above 300°C, but were found to reappear in the sample when held at 250°C. Thus the order-disorder transition occurs at 275°±25°C. The final composition of $Y_{1-x}Se$ was determined as Y/Se=0.78 by volumetric analysis (Ames Laboratory Services) using complexometry with EDTA.

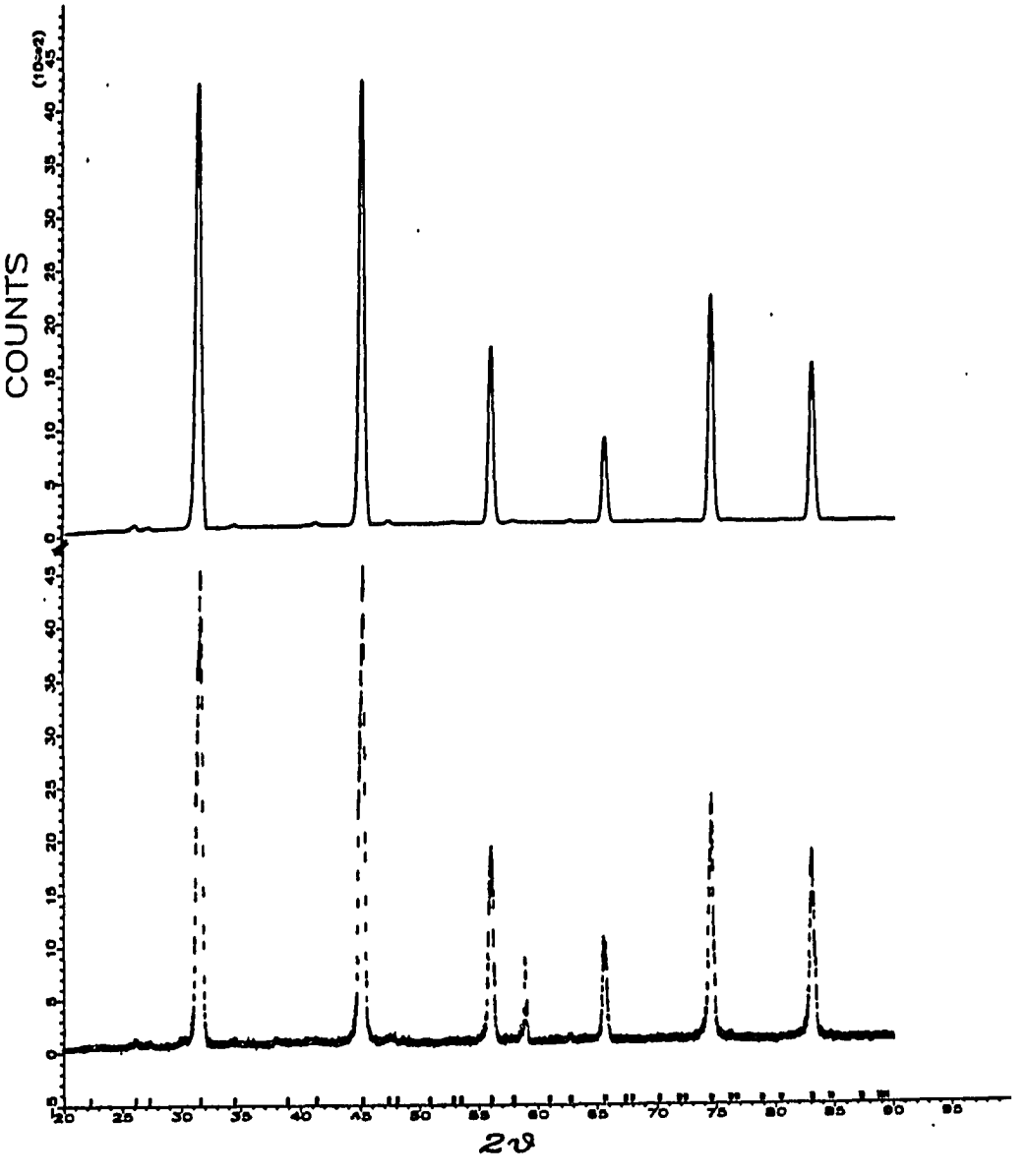

Figure 6. Comparison of calculated (top) and observed (bottom) powder diffraction for $Y_{1-x}Se$. The diffraction peaks at 30.0° and 37.9° are from Y_2O_2Se and the diffraction at 58.6° originates from the molybdenum sample holder. Vertical strokes indicate calculated Bragg peak positions

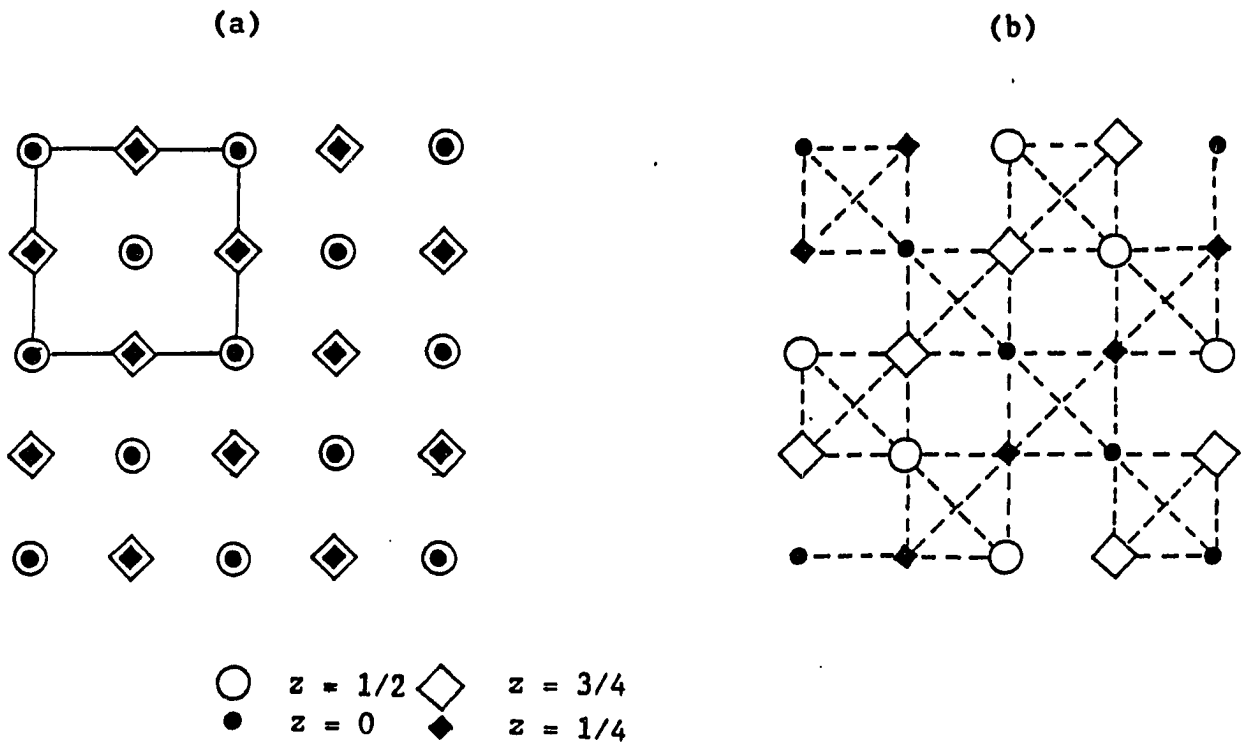

Figure 7. Yttrium positions in NaCl-type monosulfide (a) in which the parent cubic cell is indicated. Yttrium positions in idealized Ti_2C (b)

Table 11. Comparison of Fm3m and Fd3m refinement parameters

Space group	Yttrium	Selenium	Number per cell	Percent occupied	Thermal parameter(Å)
	0, 0, 0		4	92.5	0.6±1.0
Fm3m	1/2,1/2,1/2		4	32.5	-1.7±2.0
	0,1/4,1/4		24	79.0	1.6±0.5
		1/4,1/4,1/4	8	100.0	2.4±0.2
		1/4,0,0	24	100.0	2.4±0.2
Fd3m	0, 0, 0		16	59.3	1.5±0.2
	1/2,0,0		16	90.6	0.9±0.2
		1/4,1/4,1/4	32	100.0	2.4±0.2

CONCLUSION

In common with Sc and Zr monosulfides, Y monoselenide occurs with vacancies on the metal sublattice, and the fraction of sites vacant can be as large as 0.22. Also in common with these sulfides, the vacancies in defect yttrium monoselenides order at lower temperatures ($275^{o}\pm25^{o}C$ for $Y_{.78}Se$), and this ordering corresponds to the L point of the Brillouin zone. In the case of $Y_{1-x}Se$, however, the ordering corresponds to a combination of all four vectors in the star and a cubic structure with twice the NaCl-type lattice parameter results. Landau theory yields two possible structures, one with Fm3m symmetry and the other with Fd3m symmetry. The consideration of superstructure lines and thermal parameters calculated for the two models suggests that the Fd3m solution is the correct one.

SECTION IV. THE STRUCTURE OF A NEW INTERMEDIATE $Lu_{2+x}S_3$ PHASE

INTRODUCTION

Lutetium sulfide is unique among the lanthanide monosulfides in that the nonstoichiometric composition extends significantly on either side of the stoichiometric monosulfide while maintaining the NaCl-type structure. The wide range of homogeneity, which apparently results from the presence of vacancies in the sulfur or metal sublattices, extends from $LuS_{0.75}$ to $LuS_{1.30}$.[58]

During studies of the high temperature vaporization[59] of the Lu-S system a new intermediate phase, Lu_3S_4, with a structure closely related to the Sc_2S_3 structure was found between the sulfur-rich end of the monosulfide homogeneity range and Lu_2S_3.

Lutetium and scandium are both typically trivalent, and because of the lanthanide contraction, and a corresponding increase in electronegativity of lutetium, structural and high-temperature behavior of lutetium systems are similar to the corresponding scandium systems. One difference, however, is in the sesquisulfides. Whereas Lu_2S_3 has the α-Al_2O_3 type structure,[60] Sc_2S_3 has its own structure type as reported by Dismukes and White.[57,61] This structure is closely related to that of NaCl, but the unit cell is twelve times larger than the parent cubic unit cell due to a complex vacancy ordering in which one-third of scandium atomic positions are vacant. This structure is one of two variants that can result from removing one cis metal-metal edge from every $SSc_{6/2}$ octahedron. The orthorhombic dimensions of Sc_2S_3 are $a_{orth}=2a_o$, $b_{orth}=\sqrt{2}a_o$ $c_{orth}=3\sqrt{2}a_o$ where a_o is the dimension of the

parent NaCl-type sublattice, and the space group of this structure is Fddd.

The crystal structure of Lu_3S_4 was determined based on single-crystal data by Hariharan et al.[9] In this reinvestigation of the phases intermediate between lutetium monosulfide and the sesquisulfide, a new interpretation of this structure is presented based on powder diffraction data. The new intermediate phase, $Lu_{2+x}S_3$, reported here is basically isostructural with Sc_2S_3, and it is the only example of a lanthanide-sulfide with the Sc_2S_3 structure type.

EXPERIMENTAL DETAILS

The samples with initial composition range S/Lu=1.0~1.5 were prepared as previously described.

For the initial phase analysis of the samples, the x-ray powder patterns were taken using a Guinier Camera (Enraf Nonius) provided with Cu Kα radiation and a microphotometer was used to estimate the relative intensities. The phase transitions were studied using a Rigaku θ-θ diffractometer utilizing an E Buhler sample chamber and high temperature power supply. For the final data analysis the room temperature diffraction data were taken using an Elliot GX-21 rotating anode x-ray source using a vertical bent pyrolitic graphite (002) monochromator at 40KV and 200 mA. The finely ground powder sample was held in a glass capillary (diameter 0.5mm) which was rotated to minimize the effects of preferred orientation. The x-ray diffraction data were analyzed using a full-profile pattern fitting (Rietveld-type) program.[52]

RESULTS

When a sample with the composition S/Lu=1.5 was annealed at about 1400°C for several hours, the powder pattern of the quenched sample was that of the α-Al_2O_3 type. After additional heating for several hours a new phase was obtained due to loss of sulfur. The strongest lines of the diffraction pattern from this phase corresponded to an NaCl-type structure, but there were many weak extra lines. All lines were finally indexed using the Sc_2S_3 type structure. The strongest lines were relatively broad, probably due to inhomogeneity in composition.

Another set of samples with initial compositions S/Lu=1.45 and 1.50 was heated inductively for longer periods (about 60 hours) at higher temperature (1650°C) to get well homogenized, probably congruently vaporizing, samples. The Guinier powder patterns of these samples were sharper than those of the samples from lower temperature, also, instead of broadness, all the strongest substructure lines were split into 0.20~0.30(Δ 2θ) doublets. In these cases all the lines, including extra weak lines, could be indexed with the Sc_2S_3-type structure by altering the orthorhombic cell dimensions. However, when the relative intensities of the superstructure lines were fit to the Sc_2S_3-type structure, the relative intensities of the split substructure lines did not fit. For example, the first strong lines were split into lines at 28.459° and 28.667° (2θ). These lines have their origin in the parent cubic 111 reflection, and can be indexed as 220, 206 based on the orthorhombic superstructure. The intensities of those two lines should be the same in the superstructure. A careful study of the relative

intensities of all such doublets using a microphotometer indicated that two phases coexist i.e., an orthorhombic superstructure which is nearly isostructural with Sc_2S_3 and a face-centered cubic substructure.

It should be noted that good resolution is essential to study this system, since the two phases are closely related (thus there is extensive overlapping in the strongest lines), and only the relative ratios of intensities for the two phases can give the information to calculate exact compositions and shifts of atomic positions. For improved resolution, and also increased intensity the x-ray diffraction, data at room temperature were taken using an Elliot GX-21 rotating anode x-ray source and the collected data were analyzed using a Rietveld full-profile refinement program. The absorption correction appropriate to the cylindrical sample shape was made.

A fit to the combination of a superstructure with Fddd symmetry (Sc_2S_3-type) and a defect NaCl-type with Fm3m symmetry was obtained (weighted profile R factor R_w=14.65% Bragg R factor; for Sc_2S_3-type phase R_b=3.76% and for NaCl-type R_b=3.79%)

The final refined structure parameters in the orthorhombic and the cubic structures are given in Table 12 and Table 13. The calculated and observed diffraction patterns are shown in figure 8. All the strongest peaks have shoulders which originate from the orthorhombic superstructure phase, and the relative intensity ratios between these shoulders and extra weak peaks are important to determine the composition of this phase during the refinement procedure. The final composition of $Lu_{2+x}S_3$ was found to be S/Lu=1.47(3). The remainder of

the strongest lines gives the information about the cubic phase, and the refined composition of this phase yields S/Lu=1.34(2).

Table 12. Refined parameters for $Lu_{2+x}S_3$ in orthorhombic cell[a] (Overall isotropic thermal parameter: 0.49(5) $Å^2$)

Atom	Position x, y, z	Fractional occupancy
Lu (g)[b]	0.1250, 0.1250, 0.041(4)	0.96(2)
Lu (g)	0.1250, 0.1250, 0.376(4)	0.96(2)
Lu (g)	0.1250, 0.1250, 0.5416	0.13(1)
S (f)	0.1250, 0.3750, 0.1250	1.0
S (h)	0.1250, 0.3750, 0.4583	1.0

[a]Unit cell: a=10.7735(8), b=7.7053(5), c=22.873(2) Å.
[b]Wyckoff notation.

Table 13. Refined parameters for LuS_{1+x} in cubic cell[a] (Overall isotropic thermal parameter: 0.44 (4) $Å^2$)

Atom	Position	Fractional occupancy
Lu (a)[b]	0.0, 0.0, 0.0	0.75(1)
S (b)	1/2, 1/2, 1/2	1.0

[a]Unit cell: a=5.3797(1) Å.
[b]Wyckoff notation.

A sample with S/Lu=1.45 on a Mo holder was examined by high-temperature x-ray diffraction at temperatures up to 1600°C. At temperatures above 1500°C, all the peak splitting and weak

superstructure peaks disappeared and only the NaCl-type diffraction pattern was observed. Thus phase separation occurs upon cooling through about 1500°C.

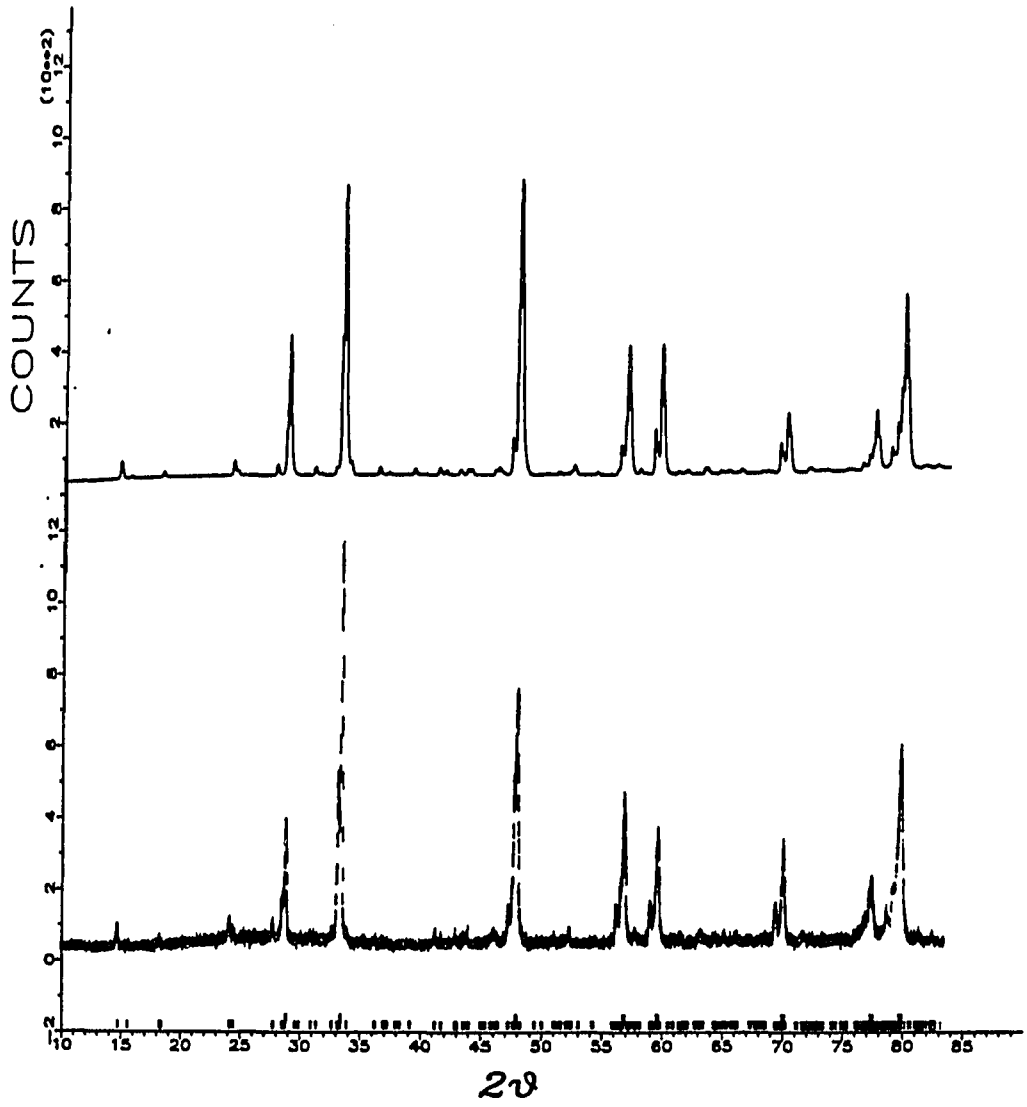

Figure 8. Comparison of calculated (top) and observed (bottom) powder diffraction for $Lu_{2+x}S_3$ and LuS_{1+x}. Vertical strokes indicate calculated Bragg-peak positions for $Lu_{2+x}S_3$ (upper) and LuS_{1+x}(Lower)

DISCUSSION

The phase with S/Lu=1.5 has the α-Al_2O_3 type structure found previously.[60] However, in the composition range between the monosulfide and the stoichiometric sesquisulfide an intermediate phase with the composition $Lu_{2+x}S_3$ and a superstructure similar to that of Sc_2S_3 is formed. The structure of $Lu_{2+x}S_3$ differs from that of Sc_2S_3 principally in small differences in the occupation of sites of the NaCl-type substructure.

The previously reported structure[9] of Lu_3S_4 is one of a number of interesting examples of ordered phases based upon defect NaCl-type solids. The results obtained here show that the single crystal upon which the Lu_3S_4 structure determination[9] was based was not characteristic of the bulk samples which were quenched from the congruently vaporizing composition. The calculated powder pattern based on the previous single-crystal result does not fit the observed pattern.

At temperatures above 1500°C, the structure is face-centered cubic and during the cooling a vacancy ordering occurs and a mixture of two phases is found at temperatures below about 1500°C. This phase separation occurs via a first order transition, since the symmetry of the superstructure does not satisfy Landau's theory of symmetry and phase transitions. It thus appears that the unusual population wave structure reported for Lu_3S_4 is appropriate to a sample in transition from the high-temperature, random vacancy distribution of hyperstoichiometric NaCl-type $Lu_{1-x}S$. It has been shown that the equilibrium phase has a small excess of Lu on sites vacant in the

Sc_2S_3-type structure, and that this phase results from S loss by vaporization from Lu_2S_3 with the α-Al_2O_3-type structure.

SECTION V. SOME OTHER SYSTEMS

THE CRYSTAL STRUCTURE OF A NEW PHASE IN THE Y-Se SYSTEM: $Y_{5-x}Se_7$

Introduction

During the investigation of the nonstoichiometric phases between YSe and Y_2Se_3, besides the vacancy ordered phase $Y_{1-x}Se$, a new phase $Y_{5-x}S_7$, was found. The crystal structure was determined by single-crystal and powder x-ray diffraction studies. The $Y_{5-x}Se_7$ phase reported here is basically isostructural with Y_5S_7,[62] but is assigned a different space group. The compound Y_5S_7 is metallic and weakly paramagnetic,[62] suggesting delocalization of electrons in addition to those in valence band of trivalent yttrium and divalent sulfur.

Experimental Details

A sample of overall composition Se/Y=1.44 was prepared by the method discussed in the synthesis section. The sample lost 0.8% of its mass during the heating.

A single crystal was selected from the blue-colored product. Intensity data were collected with an Enraf-Nonius CAD4 four-circle diffractometer and monochromated Mo K_α radiation, employing the θ-2θ scan technique up to 55^o (2θ). From the total of 1077 reflections, 585 independent reflections with $F^2 > 3\sigma(F_p^2)$ were obtained and used for structure analysis. The observed intensities were corrected for Lorentz-polarization and absorption (μ(Mo K_a)=445.3 cm^{-1}) effects. The

maximum and minimum numerical absorption correction factors were 1.503 and 0.897 respectively.

To analyze the bulk powder sample, the room-temperature powder diffraction pattern was taken using a Rigaku θ-θ diffractometer using Cu K_α radiation with a graphite exit monochromator. Least-squares structure refinement using the powder data was carried out with a Rietveld full-profile refinement program.

Structure Analysis and Discussion

The structure was solved from three-dimensional Patterson maps and refined by a full-matrix least-squares procedure (CAD4-SDP package). The initial refinement within the space group C2/m, with 19 variables including all atom positions and isotropic temperature factors, gave R=0.068 and R_w=0.096. The space group initially chosen, C2/m, was that of the isostructural Y_5S_7. One of the isotropic thermal parameters for selenium obtained from this refinement was considered abnormal. The space group Cm, with 36 variables, yielded a refinement which gave R=0.041 and R_w=0.060. To decide between Cm and C2/m, Hamilton's significance test[63] was applied, and the space group C2/m was rejected at the 0.5% level of significance. The abnormal isotropic thermal parameters of one of the selenium atoms, and the difference Fourier maps, both judged to be unreasonable in the C2/m case, provided additional evidence for rejecting C2/m.

After final refinement with numerical absorption correction and occupancy refinement, the R value was improved to R=0.036 and to

R_W=0.0491. The crystal data are summarized in Table 14 and the positional parameters and equivalent isotropic thermal parameters of the atoms are listed in Table 15. The structure is shown in Figure 9. X-ray powder diffraction data for the sample were analyzed by using the Rietveld full-profile fitting program to confirm the phase of bulk powder sample. The refinement result was in good agreement with single-crystal refinement results, but a preferred orientation characteristic of two-dimensional crystallites on a flat sample holder was found in 2 0 3 and 0 0 5 directions. The data were corrected for this preferred orientation.

Table 14. Crystal data of $Y_{5-x}Se_7$

Crystal system	monoclinic
Space group	Cm
Z	2
a(Å)	13.213(2)
b(Å)	3.9490(5)
c(Å)	12.035(1)
β, deg	104.82(1)
V, $Å^3$	697.07(1)
d(calc), g cm^{-3}	5.300(4)
Temperature(^oC)	22±1

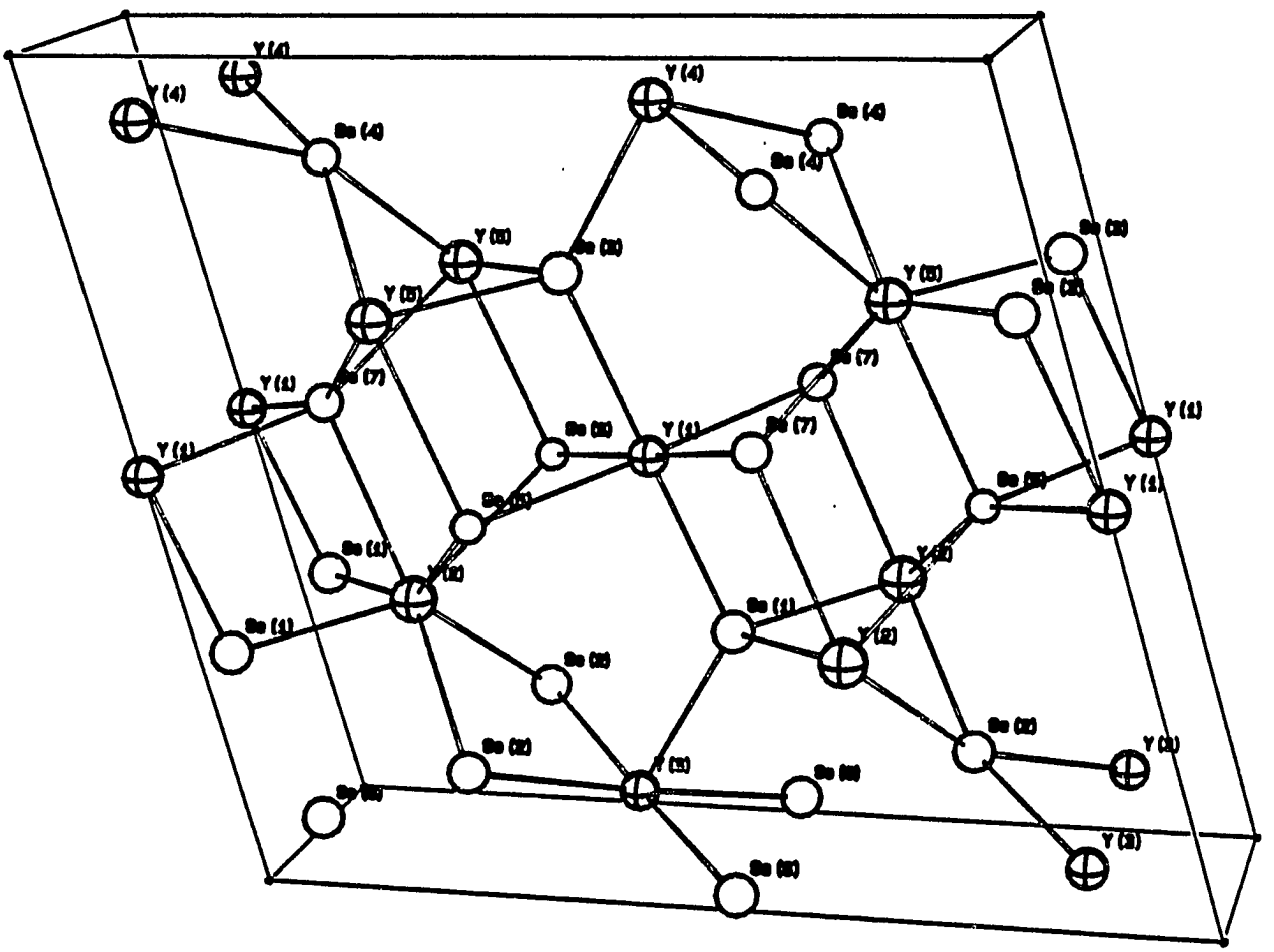

Figure 9. The structure of $Y_{5-x}Se_7$

Table 15. Atomic coordinates, equivalent isotropic thermal parameters occupancies

Atoms	x	y	z	B(Å^2)	Occupancy
Y(1)	0.000	0.000	0.500	0.738(3)	0.972(6)
Y(2)	0.1928(2)	-0.500	0.3095(2)	0.990(4)	0.958(8)
Y(3)	-0.1171(2)	0.000	0.0786(2)	0.721(4)	0.860(8)
Y(4)	0.1119(2)	0.000	-0.0741(3)	0.973(5)	0.892(8)
Y(5)	-0.1988(2)	-0.500	-0.3049(2)	1.008(4)	1.000(8)
Se(1)	0.0376(2)	0.000	0.2857(2)	0.90(4)	1.0
Se(2)	-0.2403(2)	-0.500	0.1509(2)	0.84(4)	1.0
Se(3)	-0.0380(2)	0.000	-0.2815(2)	0.86(4)	1.0
Se(4)	0.2400(2)	-0.500	-0.1462(2)	0.67(4)	1.0
Se(5)	-0.1600(2)	-0.500	0.4523(2)	0.52(4)	1.0
Se(6)	0.0106(3)	0.500	0.0182(2)	0.92(4)	1.0
Se(7)	0.1598(2)	0.500	-0.4468(2)	0.71(4)	1.0

Conclusions

The structure of $Y_{5-x}Se_7$ is basically isostructural with centrosymmetric Y_5S_7, with the different space group resulting from slight deformations from centrosymmetry. A significant new finding is the fractional occupancy of the yttrium positions providing evidence for nonstoichiometry in $Y_{5-x}Se_7$. If the mass loss at high temperature resulted from volatilization of yttrium, the overall composition of the product was Se/Y=1.46, in good agreement with the value obtained by refinement of the occupation of the yttrium positions (1.496). This nonstoichiometry yields the sesquiselenide stoichiometry that is

characteristic of a trivalent metal and a divalent non-metal. Accordingly it is possible to view the compound $Y_{5-x}Se_7$ as a sesquiselenide in the defect Y_5S_7-type structure.

In order to check the reported Y_5S_7 structure a single-crystal of Y_5S_7 was obtained and investigated. The crystal structure with C2/m symmetry was refined satisfactorily in good agreement with the former report. There were no partially occupied cationic sites, and the structures are consistent with the metallic properties of Y_5S_7 phase.

STRUCTURE REFINEMENT FOR Cr_2N

Introduction

The existence of Cr_2N with nitrogen in the octahedral interstices of hcp chromium forming a$\sqrt{3}$x$\sqrt{3}$ superstructure with $P\bar{3}1m$ symmetry was reported in 1934.[64] The results were based upon powder diffraction data. The work described here confirmed and refined the structure.

Experimental Details

A Cr_2N_{1-x} sample was prepared by heating chromium powder in a slowly flowing equivolume mixture of NH_3 and N_2 at about 1550° for 4 hours. A tungsten boat containing the powder was held in a tantalum tube, and the combination was heated inductively using a coil external to a water cooled fused silica enclosure. The temperature was estimated using an optical pyrometer.

A single crystal with an octagonal shape was selected from the silvery product. Reflection data were collected with a Rigaku AFC6 rotating anode four-circle diffractometer and monochromated Mo K_α radiation, employing the θ-2θ scan technique up to 55° (2θ). From a total of 110 reflections 55 independent reflections with $F^2 > 3\sigma (F_o^2)$ were obtained and used for structure analysis. The observed intensities were corrected for Lorentz-polarization and absorption effects.

Initially the structure was refined utilizing a full matrix least-squares procedure (Texsan-package) with the space group $P\bar{3}1m$ with all

atomic positions and isotropic temperature factors. Next only superstructure reflections were included while the chromium positions and temperature factors were fixed and the nitrogen isotropic temperature factor and multiplicity were refined to yield R=6.9%, R_w=6.90%. Finally, the superstructure reflections were added and all of the parameters were refined. The final overall R values were R=3.70%, R_w=4.59%.

Discussion

The results of the structure refinement are reported in Table 14 and 15. The results demonstrate that Cr_2N is isostructural with M_2N (M=V, Nb, Ta)[12] and confirm the previously proposed structure.[64] The chromium atoms form a hcp-type layering (ABAB$\cdots$) with nitrogen atoms in interstitial positions, two equivalent positions at z=1/2 and one position at z=0.

The refined occupation parameters indicate a slight nitrogen deficiency (N/Cr=0.46), however the value is statistically uncertain by an amount that does not preclude stoichiometric Cr_2N.

Table 16. Crystal Data for Cr_2N

Crystal System	trigonal
Space Group	$P\bar{3}1m$
Z	3
a(Å)	4.752(3)
c(Å)	4.429(4)
V($Å^3$)	86.6(1)
d_{calc} (gkm^{-3})	6.79
Temperature(^oC)	23±1

Table 17. Atomic Coordinates, Thermal Parameters, Fractional Occupancies

Atom	Position	B(Å)	Fractional Occupancy
Cr	0.333(2), 0.0, 0.2491(3)	0.33(7)	1.00(2)
N(1)	0.3333, 0.6667, 0.5	0.2(8)	0.30(4)
N(2)	0.0, 0.0, 0.0	0.1(8)	0.16(2)

VACANCY ORDERING IN Ti-O SYSTEM

According to the phase diagram for the titanium-oxygen system reported by Wahlbeck and Gilles,[65] titanium monoxide has a wide range of homogeneity with disordered vacancies and the NaCl-type structure at high temperature and ordered vacancies at low temperature. The low temperature form of TiO was observed by Watanabe et al.[13,14] by means of electron diffraction to have a monoclinic ordering of the titanium and oxygen vacancies. Further, they have found the more oxygen-rich oxide, $TiO_{1.25}$, to have a tetragonal ordering of the vacancies. A third sample of intermediate composition, $TiO_{1.19}$, was observed to be a mixture of the ordered monoclinic and tetragonal structures.

In this research, a series of samples in the composition range $TiO_{1.0}$~$TiO_{1.25}$ was examined by high-temperature and room-temperature x-ray diffraction. The samples were obtained by arc melting mixtures of Ti and TiO_2, and annealing at about 600° for 3 weeks in fused silica tubes. At room temperature, the monoclinic structure for TiO with A2/m symmetry, the tetragonal structure for $TiO_{1.25}$ with I4/m symmetry and mixtures of both structures for $TiO_{1.20}$ were verified by Rietveld full-profile refinement of diffractometer data. At high-temperatures the diffraction patterns were consistent with the NaCl-type structure. Although it was not possible to confirm the details of the ordering reactions because of extensive overlap of the strong "substructure" lines, it is concluded that these results are consistent with the reported phase diagram[65] in the $TiO_{0.9}$-$TiO_{1.3}$ region, and with Watanabe's[13,14] results.

REFERENCES CITED

1. Ashcroft, N. W.; Mermin, N. D. "Solid State Physics"; Holt, Rinehart and Winston: New York, 1976.

2. Franzen, H. F. Prog. Solid State Chem. 1978, 12, 1.

3 Franzen, H. F.; Folmer, J. C. W. J. Solid State Chem. 1984, 51, 396.

4. Franzen, H. F.; Tuenge, R. T.; Eyring, L. J. Solid State Chem. 1983, 49, 206.

5. Strotzer, E. F.; Biltz, W.; Meisel, Z. Anorg. Allg. Chem. 1939, 242, 249.

6. Jellinek, F. Ark. Kem. 1962, 20, 447.

7. Conard, B. R.; Franzen, H. F. High Temp. Sci. 1971, 3, 49.

8. Conard, B. R.; Franzen, H. F. "Chemistry of Extended Defects in Non-Metallic Solids"; L. Eyring and M. O'keeffe, Eds.: North Holland: Amsterdam, 1970.

9. Hariharan, A. V.; Powell, D. R.; Jacobson, R. A.; Franzen, H. F. J. Solid State Chem. 1981, 36, 148.

10. Brauer, G; Esselborn, R. Z. Anorg. Allg. Chem. 1961, 309, 151.

11. Guard, R. W.; Savage, J. W.; Swarthout, D. G. Trans. Metall. Soc. AIME. 1967, 239, 643.

12. Christensen, A. N. Acta Chem. Scand. 1976, A30, 219.

13. Watanabe, D.; Terasaki, O.; Jostsons, A.; Castles, J. R. "Chemistry of Extended Defects in Non-Metallic Solids"; L. Eyring and M. O'Keeffe, Eds.: North Holland: Amsterdam, 1970.

14. Watanabe, D.; Terasaki, O.; Jostsons, A.; Castles, J. R. J. Phys. Soc. Jpn. 1968, 25, 292.

15. Roth, W. L. Phys. Rev. 1958, 110, 1333.

16. Moodenbaugh, A. R.; Johnston, D. C.; Viswanathan, R.; Shelton, R. N.; Delong, L. E.; Fertig, W. A. J. Low Temp. Phys. 1978, 33, 175.

17. Johnston, D. C.; Moodenbaugh, A. Phys. Lett. 1972, 41A, 447.

18. Aschermann, G.; Frederich, E.; Justi, E.; Kramer, J. Phys. Z. 1941, 42, 349.

19. Giorgi, A. L.; Szklarz, E. G.; Storms, E. K.; Bowman, A. L.; Matthias, B. T. Phys. Rev. 1962, 125, 837.

20. Willens, R. H.; Buehler, E.; Matthias, B. T. Phys. Rev. 197, 159, 327.

21. Banus, M.D. Mat. Res. BuLL. 1968, 3, 723.

22. Doyle, N. J.; Hulm, J. K.; Jones, C. K.; Miller, R. C.; Taylor, A. Phys. Lett. 1968, 26A, 604.

23. Toth, L. E. "Transition Metal Carbides and Nitrides"; Academic Press: New York, 1971.

24. Pessall, N; Hulm, J. K. Physics (Long Island City, NY) 1966, 2, 311.

25. Pessall, N; Gold, R. E.; Johansen, H. A. J. Phys. Chem. Solids 1968, 29, 19.

26. Burdett, J. K.; Hughbanks, T. J. Am. Chem. Soc. 1984, 106, 3101.

27. Franzen, H. F.; Merrick, J. A. J. Solid State Chem. 1980, 33, 371.

28. Huisman, L. M.; Carlsson, A. E.; Gelatt, C. D., Jr.; Ehrenreich, H. Phys. Rev. B 1980, 22, 991.

29. Denker, S. P. J. Less-common Met. 1968, 14, 1.

30. Goodenough, J.B. Phys. Rev. B 1972, 5,2764.

31. Nakahara, J. F.; Ph.D. Dissertation, Iowa State University, Ames, IA, 1984.

32. Tremel, W.; Hoffmann, R. J. Less-common Met. 1986, 116, 113.

33. Tremel, W.; Hoffmann, R. J. Am. Chem. Soc. 1986, 108, 5174.

34. Franzen, H. F.; Haas, C.; Jellinek, F. Phys. Rev. B 1974, 10, 1248.

35. Beck, L. H.; Smith, C. S. Trans. AIME 1952, 194, 1079.

36. Landau, L. D.; Lifschitz, E. M. "Statistical Physics"; Pergamon: London, 1962, Chapter 14.

37. Franzen, H. F. "Physical Chemistry of Inorganic Crystalline Solids"; Springer Verlag: Heidelberg, 1986.

38. Tolédano, J.-C.; Tolédano, P. "The Landau Theory of Phase Transitions"; World Scientific: Singapore, 1987.

39. Haas, C.; Phys. Rev. A 1965, 140, 863.

40. Kim, S. J.; Nguyen, T.-H.; Franzen, H. F. J. Solid State Chem. 1987, 70, 80.

41. Kovalev, O. V.; "Irreducible Representations of the Space Groups"; Translated by A. Murray Gross, Gordon and Breach: New York, 1965.

42. Franzen, H. F. J. Less-common Met. 1989, in press.

43. Rooksby, H. P. Acta Crystallogr. 1948, 1, 226.

44. Willis, B. T. M.; Rooksby, H. P. Acta Crystallogr., 1953, 6, 827.

45. Tombs, N. C.; Rooksby, H. P. Nature, 1950, 165, 442.

46. Eddine, M. N.; Sayetat, F.; Felix, E. Compt. Rend. Hebd. Seances Acad. Sci., Ser B. 1969, 269, 574.

47. Pauling, L.; Soldate, A. Acta Crystallogr. 1948, 1, 212.

48. Kim, S.-J.; Franzen, H. F. J. Less-common Met. 1988, 144, 117.

49. Hahn, H.; Harder, B.; Mutschke, U; Ness, P. Z. Anorg. Allg. Chem. 1957, 292, 82.

50. Rabenau, A.; Schulz, H.; J. Less-common Met. 1976, 48, 89.

51. Kim, S.-J.; Franzen, H. F. J. Less-common Met. 1988, 143, 339.

52. Kim, S.-S. Ph.D. Dissertation, Iowa State University, Ames, IA, 1986

53. Wiles, D. B.; Young, R. A. J. Appl. Crystallogr. Chem. 1981, 14, 149.

54. McTaggert, F. K; Wadsley, A. D. Australian J. Chem. 1958, 11, 445.

55. Nguyen, T.-H. Ph.D. Dissertation, Iowa State University, Ames, IA, 1980.

56. Kennett, H. M.; Rudee, M. L. Phil. Mag. 1977, 35, 129.

57. Dismukes, J. P.; White, J. G. Inorg. Chem., 1965, 4, 970.

58. Franzen, H. F.; Hariharan, A. V. J. Solid State Chem. 1978, 26, 189.

59. Franzen, H. F.; Hariharan, A. V. J. Chem. Phys. 1979, 70, 4907.

60. Flahaut, J.; Domange, L.; Pardo, M. Compt. Rend. 1963, 256, 1793.

61. Dismukes, J. P.; White, J. G. Inorg. Chem. 1964, 3, 1220.

62. Adolphe, C. Ann. Chim. 1965, 10, 271.

63. Hamilton, W. C. Acta Crystallogr. 1965, 18, 502.

64. Eriksson, S. Jernkontorets Annaler. 1934, 118, 530.

65. Wahlbeck, P. G.; Gilles, P. W. J. Am. Ceram. Soc. 1966, 49, 180.

ACKNOWLEDGEMENTS

I would like to express my gratitude to Dr. Fritz H. Franzen, my major professor, for his advice and guidance throughout the course of this study. This research work was accomplished very effectively due to his valuable insight and suggestions. I enjoyed my experience of working with him, for I always learned something from our contact.

Also, I would like to thank Jim Anderegg for his help with the laboratory work. To the present group members and Shirley Standley, I thank you for your friendship.

I wish to thank my parents and brothers in Korea who understood and supported me while studying abroad.

Special thanks to my husband and my lovely daughter Alm Sarah who accompanied me in those long days to see the outcome of this work.

This work was performed at Ames Laboratory under contract No. W-7405-eng-82 with the U. S. Department of Energy. The United States government has assigned the DOE Report number IS-T 1389 to this thesis.